Liquid Crystals
Publication details, including instructions for authors and subscription information:
http://www.informaworld.com/smpp/title~content=t713926090

The electro-optical characteristics and applicability evaluation of a photo-induced vertical alignment negative-type liquid crystal/photo-curable acrylic pre-polymer mixture system mixed with chiral smectic A phase liquid crystal

Czung-Yu Ho[a]; Jiunn-Yih Lee[a]
[a] Department of Materials Science and Engineering, National Taiwan University of Science and Technology, Taiwan, Republic of China

Online publication date: 15 January 2011

To cite this Article Ho, Czung-Yu and Lee, Jiunn-Yih(2011) 'The electro-optical characteristics and applicability evaluation of a photo-induced vertical alignment negative-type liquid crystal/photo-curable acrylic pre-polymer mixture system mixed with chiral smectic A phase liquid crystal', Liquid Crystals, 38: 1, 65 — 86
To link to this Article: DOI: 10.1080/02678292.2010.527381
URL: http://dx.doi.org/10.1080/02678292.2010.527381

Liquid Crystals,
Vol. 38, No. 1, January 2011, 65–86

Taylor & Francis
Taylor & Francis Group

The electro-optical characteristics and applicability evaluation of a photo-induced vertical alignment negative-type liquid crystal/photo-curable acrylic pre-polymer mixture system mixed with chiral smectic A phase liquid crystal

Czung-Yu Ho* and Jiunn-Yih Lee

Department of Materials Science and Engineering, National Taiwan University of Science and Technology, Taiwan, Republic of China

(*Received 14 August 2010; final version received 23 September 2010*)

In this study, we have investigated newly synthesised chiral smectic A (SmA*) liquid crystals (LCs) with a lactic acid structure with polarised optical microscopy (POM). We started cooling from the clear point until a SmA* phase emerged as the temperature dropped to the range 55.7–88.6°C. At this point, the alignment of the LC molecules resulted in a homeotropic texture. To take advantage of this characteristic, we then mixed the SmA* LC into a negative dielectric anisotropy nematic-type liquid crystal (NLC)/photo-curable acrylic pre-polymer mixture system (the NLC mixture system) with photo-induced vertical alignment, to realise the vertical alignment effect among the NLC molecules. This multi-component LC mixture system gave rise to a special, unknown twist grain boundary AX (TGB_{AX}*) phase with rather broad temperature range, which maintained its helix structure even after crystallisation. In addition, we also utilised the electrical field induced molecular tilt effect (the electroclinic effect) within the SmA* LC to improve the response time of the LC device and gray-scale capability of the NLC mixture system. We further observed this multi-component LC mixture system after ultraviolet light irradiation treatment with POM, to investigate the alignment of the LC molecules, device display and electro-optical properties.

Keywords: liquid crystal; homeotropic texture; twist grain boundary; electroclinic effect

1. Introduction

In the liquid crystal display (LCDs) industry, extensive efforts have been devoted to the study and development of alignment techniques for LC molecules. The key purpose of LC alignment is to arrange the LC molecules in a specific direction in accordance with the modular design of devices, so as to realise dynamic control of the display.

The traditional method for LC molecule alignment is to coat a layer of organic polymer film, e.g. polyimide (PI), on a conductive glass substrate coated with a very thin layer of indium-tin oxide (ITO). Thereafter, the surface of the PI film is unidirectionally rubbed with a velvet cloth (e.g. cotton, nylon, rayon, etc.) [1] to extend and thus orientate the polymer main chains along a specific direction, thereby creating micro-grooves along which the LC molecules will naturally be aligned. The advantages of this technique are that the rubbing alignment method has extremely short operation time, can be performed at room temperature and is eminently suited for mass production. Nevertheless, there also exists many drawbacks [1, 2], e.g. organic polymer materials such as PI have high polarity and are highly water absorbent, meaning that they deteriorate rapidly during storage and transportation, thereby resulting in uneven alignment. Additionally, dust particles, electrostatic remains, brush marks, etc. from the rubbing alignment process often lead to defective devices and thus a decrease in the yield rate of the production [1].

Therefore, numerous non-rubbing alignment methods have been developed to counter the problems inherent in traditional contact mode mechanical rubbing processes and realise LC molecule alignment, e.g. photo-alignment [3–29], ion-beam alignment [13, 25, 30–35], Langmuir–Blodgett (LB) films [5, 36, 37], plasma treatment [38–40] and nano-imprinting [41–46], etc.

Our prior studies on non-contact mode photo-induced vertical alignment methods [47–49] were primarily based on the principles and theories of the phase separation composite film (PSCOF) technology [50], as well as related reports [51–65] presented by Kumar *et al.* from Kent State University in 1999, for the extension and application of the LC/photo-curable acrylic pre-polymer mixture systems to fabricate vertical alignment (VA) mode LC devices and completely do away with pre-processing of the PI, improve yield and boost production.

However, before the PSCOF method was proposed by Kumar *et al.*, numerous non-contact mode process technologies such as the LC/photo-curable pre-polymer had already been proposed. For example, photo-polymerisation induced phase separation

*Corresponding author. Email: ketcer2009@gmail.com

ISSN 0267-8292 print/ISSN 1366-5855 online

DOI: 10.1080/02678292.2010.527381
http://www.informaworld.com

(PIPS) [66–71] methods for the study and application of LC devices, such as polymer stabilised cholesteric texture (PSCT), polymer network stabilised liquid crystal (PNSLC), polymer dispersed liquid crystal (PDLC) [72–125], etc. were subjects of extensive research. The morphology of the polymer structure varied widely depending on the process parameters such as the photo-curable pre-polymer structure, the mixing ratio between the LC and photo-curable pre-polymer, the cell thickness, the environment temperature, the ultraviolet (UV) light irradiation intensity and UV light irradiation times. Such significant variations in the polymer structure morphology thus obtained necessarily led to differences in the operation modes and applications of these LC devices [47–49, 53, 60, 84, 86, 90, 94, 95, 101, 102, 105, 109, 113].

In 2000, Kumar *et al.* presented the relevant theories and experiments in a paper [53] outlining how a LC/photo-curable pre-polymer mixture system, after UV light irradiation induced phase separation, exhibited a strong dependence of the polymer structure morphology on the rate of photo-polymerisation. Thereafter, in 2005, Kumar *et al.* further varied process parameters such as the UV light irradiation intensity, curing temperature, cell thickness, etc. in accordance with the theoretical framework and empirically demonstrated the effective control of these parameters in yielding polymer films (PSCOF or PDLC films) with different structure morphologies [60]. Therefore, in our previous studies [47–49], we successfully demonstrated the fabrication of vertical alignment copolymer film (VACOF) LC devices with double VA mode layers based on their works.

Furthermore, after fabricating a LC with smectic A phase with lactic acid structure (two chiral smectic A phase, SmA*) and filling it into a LC cell with no polymer alignment, we observed complete vertical alignment of the LC molecules (homeotropic texture) under crossed polarised optical microscopy (POM) [126]. Therefore, in this study, we have attempted to mix SmA* LC material into a negative dielectric anisotropy nematic-type liquid crystal (NLC)/photo-curable acrylic pre-polymer mixture system (presented in a previously published study) not only to achieve LC molecule vertical alignment in the original system (the NLC mixture system), but also to strengthen the surface anchoring energy of the original VACOF, enhance the response time of the LC device and improve its gray-scale performance.

Over the course of the experiment, we also found that this multi-component LC mixture system yielded a special, unknown twist grain boundary AX phase ($TGB_{AX}{}^{*}$). In general, TGB phases occur in cholesteric-type liquid crystal or smectic-type liquid crystal with high chirality and exhibit filament texture or Grandjean (planar texture) under crossed POM. Although this LC phase with special configuration was formally discovered in 1989 by Goodby *et al.* [127, 128], P. G. de Gennes had presented the similarity between the smectic LC phase and the superconductor as early as 1972, notably how the effect of the chirality on the smectic phase is akin to that of the magnetic field on superconductors [129]. In 1988, Renn and Lubensky proposed the existence, between the cholesteric phase and smectic phase, of a LC phase resembling the Type II Abrikosov flux lattice in superconductors, specifically known as the twist grain boundary (TGB) phase [130]. Furthermore, a review of the literature will reveal that the majority of LC materials exhibiting the TGB phase are ferroelectric or cholesteric LC with high chirality [131–140]. One will also find the TGB phase or blue phase (BP) in at least two kinds of LC mixtures [141–145]. In addition, there have been reports where the TGB phase was observed after metals were blended with the LC [138]. In 1992, Renn and Lubensky further proposed the theory of a tilt $TGB_C{}^{*}$ phase [146, 147], where, in contrast to the smectic A and smectic C phases, the TGB phase can be further sub-categorised into two sub-stable LC phases: namely $TGB_A{}^{*}$ and $TGB_C{}^{*}$, the possible configuration structures of which are shown in Figure 1. The most significant difference between the two is that the long axis of the LC molecules lies perpendicular to the layer plane for the $TGB_A{}^{*}$ phase, whereas the long axis of the LC molecules lies at a tilt angle to the direction perpendicular to the layer plane for the $TGB_C{}^{*}$ phase [148]. The existence of the $TGB_C{}^{*}$ phase was first experimentally verified by the Bordeaux research team [149], and within a few years, other studies reported the emergence of the $TGB_C{}^{*}$ phase in other materials during the cooling process. Some materials exhibited only the $TGB_A{}^{*}$ phase or $TGB_C{}^{*}$ phase [127, 128, 135, 150–152] whereas yet others simultaneously exhibited both the $TGB_A{}^{*}$ phase and $TGB_C{}^{*}$ phase [149, 153, 154], giving rise to a thrust of research on frustrated phases [140, 155, 156] and several related experiments and studies of their characteristics [157–168]. The TGB phase structure continues to be the focus of extensive and concerted research efforts and a field which we are keen to probe in depth.

SmA* LC exhibits the electroclinic effect [126, 169–173], i.e. when an electrical field (E) is applied, the LC molecules will follow the direction of E and be inclined at a tilt angle from the original normal of the molecules, due to their dipole moments. This is one example of the phenomenon of spontaneous polarisation (PS). When an external electrical field is applied, the PS phenomenon of the material itself will result in alignment with the electrical field. Therefore, this

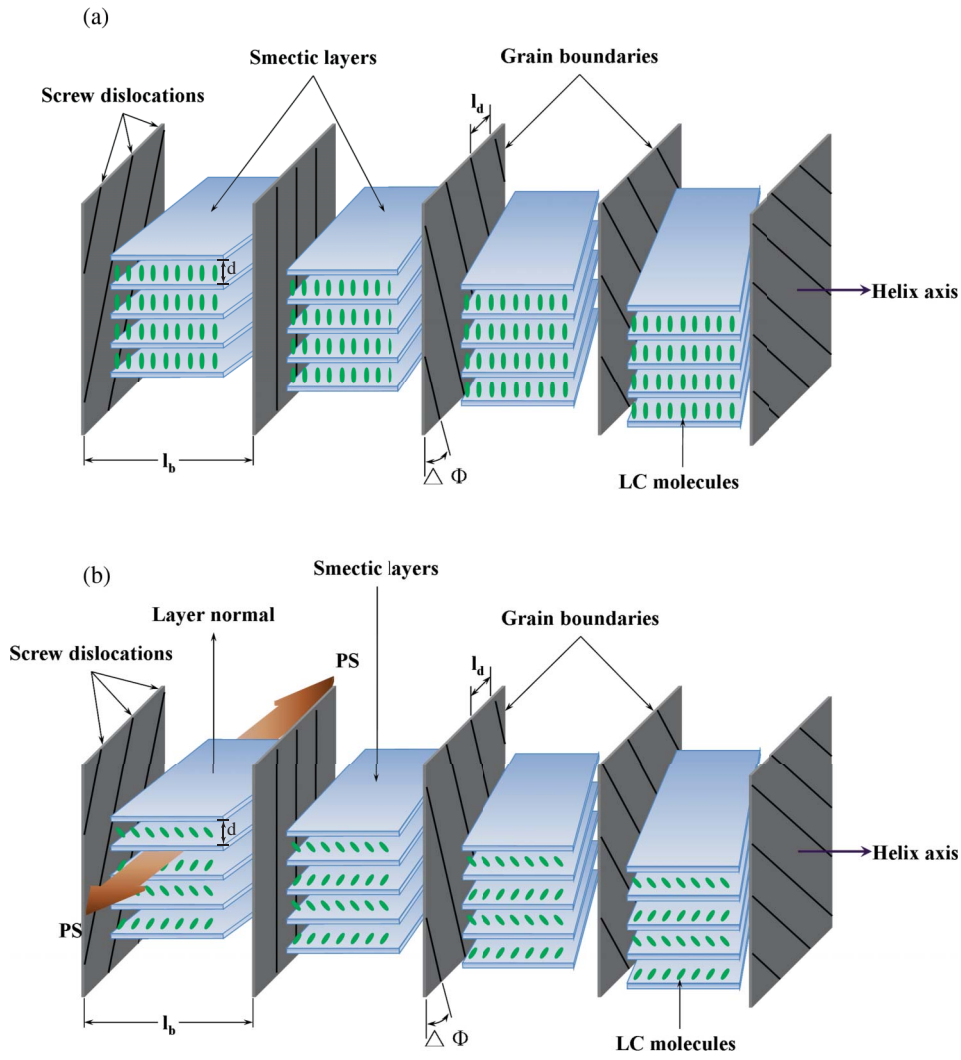

Figure 1. Special configurations of the (a) TGB_A^* phase and (b) TGB_C^* phase picture. (The presence of a grain boundary allows the rotation of the layer normal by a finite angle $\Delta\Phi$. Blocks of SmA layers of spacing d are separated by regularly spaced twist grain boundaries separated by a distance I_b. The distance between screw dislocations within a grain boundary is I_d.)

physical phenomenon has captured the attention of many researchers due to its potential for creating a switch between the bright and dark states. The electroclinic effect of the SmA* LC offers a faster response time than that in ferroelectric LC, and further allows for the gray-scale capability of adjusting the amount of light passing through [173, 174], on top of an excellent, stable chemical structure. The speedy tilt angle conversion enables applications in display technology [175]. In summary, we hope to leverage the advantages of the SmA* LC materials to improve electro-optical characteristics such as the gray-scale properties and response time of the original system (the NLC mixture system), and perform an initial feasibility evaluation, application and test for several LC devices with a multi-component LC mixture system.

2. Experiment

2.1 Materials and introduction of liquid crystal mixture systems

First of all, we used the SmA* phase LC materials, which we had synthesised in our laboratory, to complement a LC mixture system (the original NLC mixture system) with non-contact mode photo-induced VA mode effect. The chemical structure of the SmA* LC materials, as shown in Figure 2, consists of a molecular core containing three benzene rings. The main body of the LC molecule is the biphenyl ring connected to a single benzene ring by ester groups (–COO–), and is in turn connected to the two chiral centres with oxygen groups (–O–), which enhance the chemical stability. Furthermore, to avoid the meso

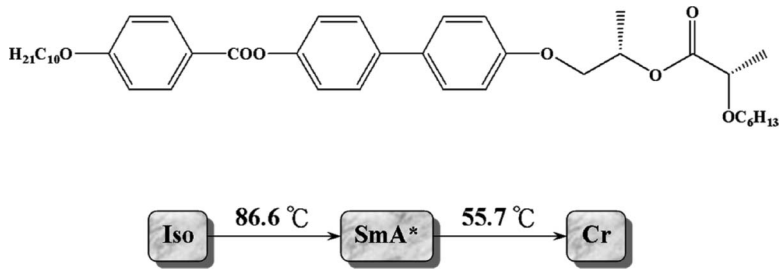

Figure 2. The chemical structure and phase transition temperature variation of the pure two SmA* phase liquid crystal material.

state, the chiral centres are set in the (S,S) direction [176]. To enhance the stability of the SmA* LC and lower the clear point (equivalent to the isotropic temperature, T_{iso}), we designed a longer terminal group soft segment (with alkoxy group carbon number of 10) and a chiral group soft segment (with alkoxy group carbon number of 6). From the structural design and thermal analysis (differential scanning calorimeter, DSC) of the LC molecules, we determined that the SmA* LC phase encompasses a very wide temperature range, and possesses a large electrical field induced molecular tilt angle (~10°), fast response time and gray-scale adjustment capability [126].

The key reason for mixing SmA* LC materials into the negative dielectric anisotropy NLC mixture system, other than the aforementioned characteristics desired, was that when the material was filled into an empty cell without a polymer alignment layer (with cell thickness $d = 4$ μm), the LC molecules would be vertically aligned onto the surface of the ITO glass substrate, thereby exhibiting a uniformly dark state under the crossed POM [126]. Therefore, the objective of the experiment was to add a trace amount of SmA* LC into the NLC mixture system and observe the effect on the LC molecule arrangement of the original system, and ascertain if we could improve the electro-optical properties. The chemical structures of the photo-curable acrylic pre-polymer and photo-initiator used for the NLC mixture system are shown in Figure 3.

2.2 *Preparation of the NLC and NLC-SmA*/photo-curable acrylic pre-polymer mixture systems*

In previously discussed LC mixture systems [47–49], we mixed alkyl long carbon chain acrylic pre-polymer A (we utilised in this experiment organic polymers with side chain structure similar to that of PI to simulate the traditional rubbing process used in the fabrication and long carbon alkyl side chain (alkyl carbon number 10, SeaEn Special Material Co.) to effect vertical alignment of the LC molecules), main chain type biphenol acrylic pre-polymer B (as the pseudo-organic polymer film main structure for grafting with acrylic pre-polymer

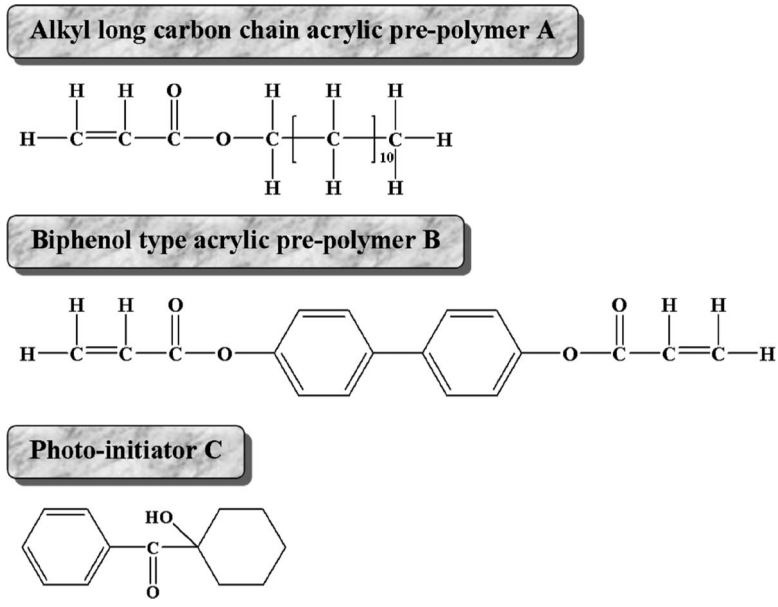

Figure 3. The chemical structure of the photo-curable acrylic pre-polymer and photo-initiator LC mixture system.

Table 1. Component and weight percentage ratios of each LC mixture system.

	LC material (wt%)		Acrylic pre-polymer (wt%)		Photo-initiator (wt%)
LC mixture system	Pure NLC	Pure SmA*	A[a]	B	C
NLC	97.8	-	1.8	0.3	0.1
NSLC	95.6	2.2[b]	1.8	0.3	0.1

Notes: [a] Alkyl carbon number of acrylic pre-polymer A is 10.
[b] In the NSLC mixture system, the total weight percentage of the SmA* LC material, acrylic pre-polymer A and B, and photo-initiator is the same (SmA*:A + B + C = 1:1).

A, SeaEn Special Material Co.) and photo-initiator C (which creates free radical polymerisation reactions after the UV light irradiation process, Ciba Specialty Chemicals Co.), etc. with room-temperature type negative dielectric anisotropy NLC ($\Delta\varepsilon = -4.1$, $\Delta n = 0.0899$, $\eta_1 = 0.21$ kg m^2 s, $K_{\text{eff}} = 18.1$ pN, Merck) to obtain the NLC mixture system. Also, during the course of the experiment, we found that when the alkyl carbon number of the acrylic pre-polymer A was 10, LC devices with the best electro-optical properties were obtained [48]. For this reason, we continued to use previously fabricated NLC mixture systems, and added a chiral SmA* phase LC to obtain the NLC-SmA*/photo-curable acrylic pre-polymer mixture system (NSLC mixture system) for the study. The NLC was the main component of the LC mixture system investigated in this experiment, and the mixing ratios of each component are shown in Table 1.

The mixing ratio of SmA* was equivalent to the total mixing ratios of the acrylic pre-polymer A (1.8 wt%), B (0.3 wt%) and photo-initiator C (0.1 wt%) in the original NLC mixture system (A+B+C = 2.2 wt%). Therefore, for the NSLC mixture system, we attempted to measure the electro-optical and display properties of the LC devices under the 1:1 ratio (SmA*: A+B+C = 1:1).

The NLC and NSLC mixture solutions were obtained by heating to approximately 40°C above the clear point (isotropic temperature) of the LC, in conjunction with ultrasonic vibration and stirring for about 1 hour. The LC mixture solutions were kept stable in a homogeneously isotropic phase at room temperature, and injected by capillary action under vacuum to fill an empty cell with 4 μm ball-shaped glass fibre spacers.

2.3 Photo-polymerisation induced phase separation process and UV-curing behaviours of the NLC and NSLC mixture systems

There are a myriad of factors which can affect the polymer film morphology, e.g. cell thickness, curing temperature, UV light irradiation intensity, UV light irradiation times, etc., all of which have different effects on the PIPS rate of the photo-curable pre-polymer and give rise to polymer films (PSCOF or PDLC films) [53, 60] with different external morphologies, characteristics and applications. Therefore, to obtain a VACOF structure morphology with smooth surface, the sample temperatures of the NLC and NSLC mixture systems were kept at 90°C (the isotropic temperature of the LC) using a Mettler FP-82HT hot stage and FP-90 central process during the UV light irradiation at fixed UV light intensity (~5 mW cm^{-2}) [47–49]. After completion of the PIPS process (Figure 4), the NLC and NSLC mixture cells were slowly cooled to room temperature.

In addition, we prepared the NLC and NSLC mixture solutions with a methanol solvent concentration of 3.3×10^{-6} mol L^{-1}, and made use of a ultraviolet-visible (UV-Vis) absorption spectrometer (VARIAN, Inc., Cary 100 Conc.) to measure variations in the absorption values ($\lambda_{\max}$) of the two LC mixture systems during UV light irradiation (from 0 to 30 min), before converting them to the UV conversion percentage (CP) [48, 49] of the materials, to ascertain the degree of VACOF polymerisation, the ideal UV light irradiation time, etc.

2.4 Thermal properties analysis and observations

We hoped to understand the effect of mixing pure negative dielectric anisotropy NLC with materials such as SmA*, photo-curable acrylic pre-polymer A and B, a photo-initiator, etc. on the LC phase transition temperature. The phase transition temperature (°C) and enthalpies (J g^{-1}) of the NLC and NSLC mixture compounds were determined by DSC (Perkin–Elmer DSC 4000). The phase transition temperatures were read at their maximum endothermic and exothermic peaks ($T_{\text{endo, max}}$ and $T_{\text{exo, max}}$). All LC mixture compounds were examined at the heating and cooling rate of 5°C min^{-1} under a nitrogen atmosphere. Moreover, the transition temperatures were obtained from the specified second heating and cooling scans.

The liquid crystalline texture of the NLC and NSLC mixture compounds were observed with POM (Olympus Optical Co., Ltd., Models BHSP-2, BX-51)

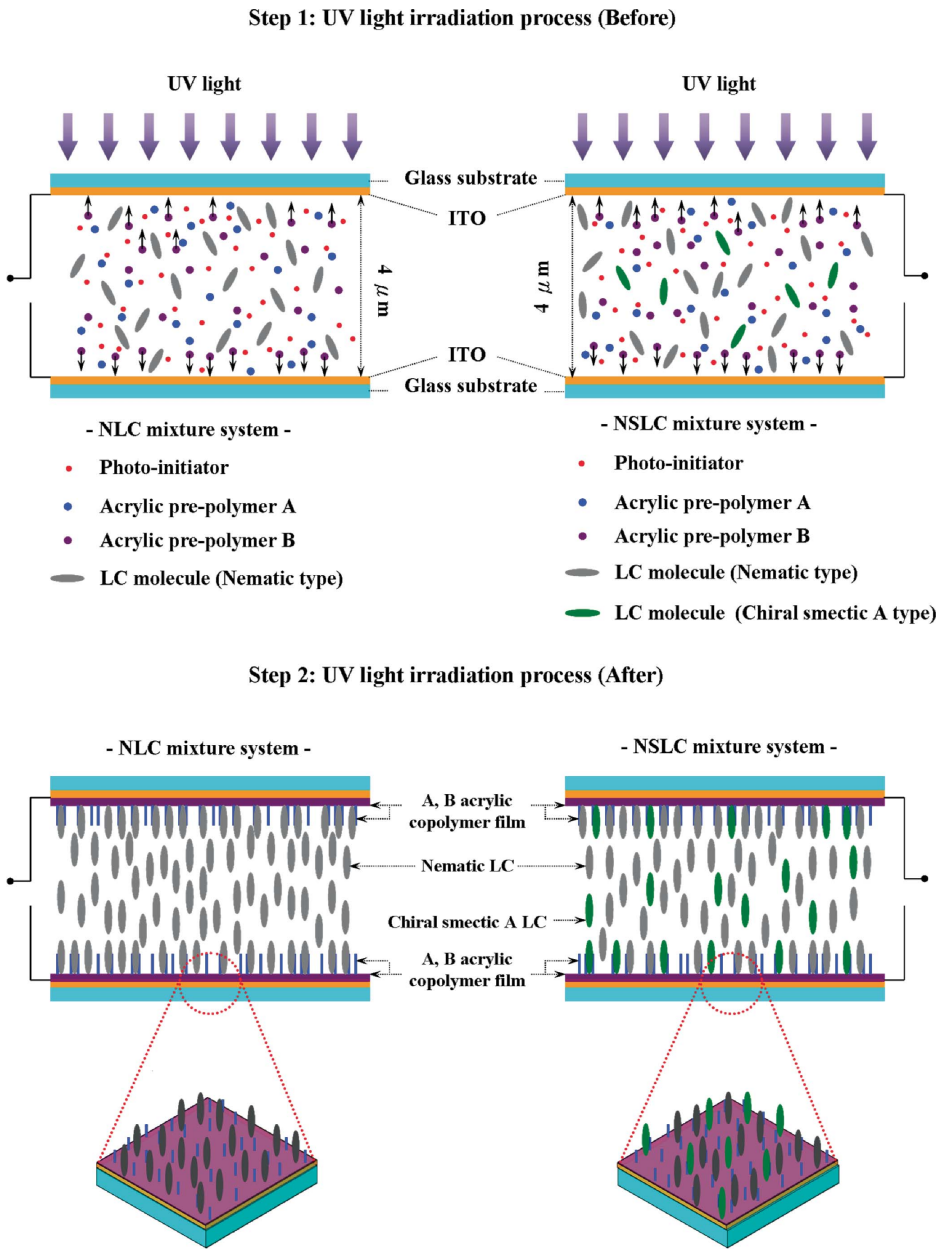

Figure 4. The NLC and NSLC mixture cells after UV light irradiation, with the formation of the double layers VACOF due to phase separation.

coupled with a Mettler FP-82HT hot stage and FP-90 central process. The setup is as shown in Figure 5.

2.5 *Electro-optical properties of the LC mixture systems*

2.5.1 Transmittance, threshold voltage, driving voltage and saturation voltage

For measuring the transmittance of the LC mixture cells, we primarily made use of white light as the incident light source [47–49], and the setup for measuring properties such as the transmittance threshold voltage (V_{th}), driving voltage (V_{on}), saturation voltage (V_{sat}), etc. is shown in Figure 6.

First, we placed the LC mixture cell under the POM with cross polarisers ($V = 0$), and defined the transmittance to be 0%; thereafter, we applied the saturation voltage ($V = V_{sat}$) and defined the state with maximum brightness as 100%, for the purpose of calibration. Subsequently, we placed the LC mixture cell under the crossed polarisers of the POM and applied an AC electrical field (0–10 V, 60 Hz, square wave) with a waveform generator (Yokogawa Electric Co., Ltd., Models AG1200). The

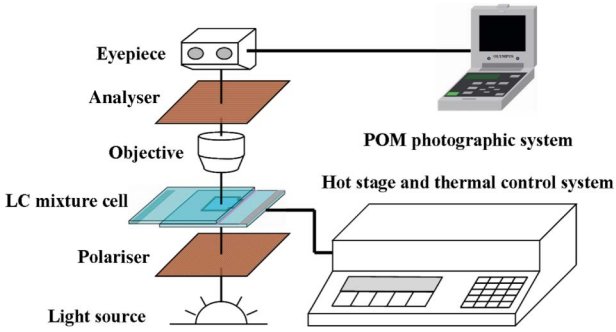

Figure 5. Setup for observing the liquid crystalline texture of the LC mixture cells with POM.

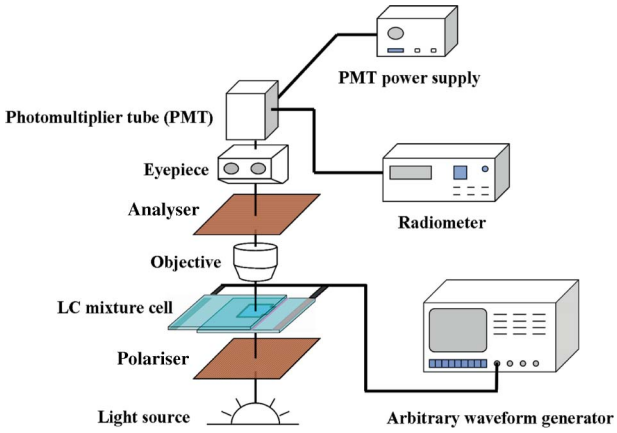

Figure 6. Setup for measuring the transmittance, threshold voltage (V_{th}), driving voltage (V_{on}) and saturation voltage (V_{sat}) of the LC mixture cells.

light signal received by a PhotoMultiplier Tube (PMT, International light, SED038) was then converted via a Radiometer (International Light Inc., Models IL1700) into numerical values to study the variation of the transmittance with a slowly increasing voltage [177]. From the transmittance vs. applied voltage curve, we can further obtain the threshold voltage (V_{th}, defined to be the voltage when the transmittance reached 10%), driving voltage (V_{on}, defined to be the voltage when the transmittance reached 90%) and saturation voltage (V_{sat}, defined to be the voltage when the transmittance reached 100% (maximum)) of all the LC mixture cells. When the tilt direction of the LC molecules inside the LC mixture cell under the influence of the electrical field ($V = V_{sat}$) reached 45 degrees with the cross polarisers, we obtained the maximum transmittance. The transmitted light intensity, I, is given by [178, 179]

$$I = I_0 \sin^2 2\theta \sin^2(\pi d \Delta n(V)/\lambda), \qquad (1)$$

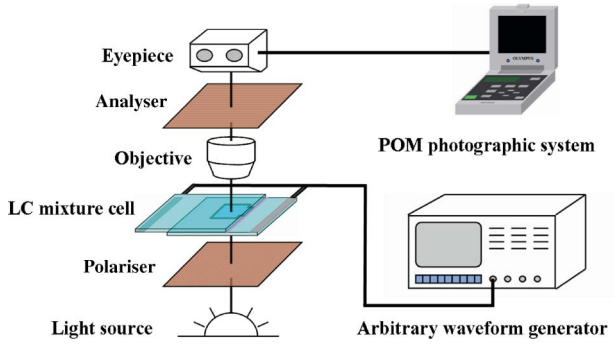

Figure 7. Setup for observing the display condition of the LC mixture cells with POM.

where I_0 is the incident light intensity, θ is the angle between the polarisation direction of the incident light and the long axes of the LC molecules, and d and $\Delta n(V)$ are the cell thickness and birefringence under a voltage V, respectively. Here, I/I_0 is the transmittance (T), $d\Delta n(V)$ is the retardation R of the LC and λ is the wavelength of the incident light.

Furthermore, under the POM with crossed polarisers, due to the electrically controlled birefringence (ECB) effect [180–183], we can observe the dark and bright state display conditions before ($V = 0$, the long axis of the LC molecules will be vertically aligned to the ITO glass substrate surface) and after ($V = V_{sat}$, the short axis of the LC molecules and electrical field direction will be parallel to each other) a voltage is applied to the LC mixture cell. The setup is as shown in Figure 7.

2.5.2 *Response time*

Figure 8 shows the setup for measuring the response time of the LC mixture cell [177]. We used a He-Ne

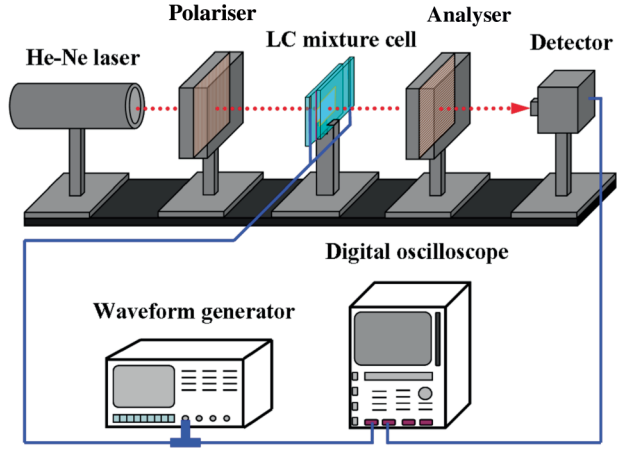

Figure 8. Setup for measuring the response time of the LC mixture cells.

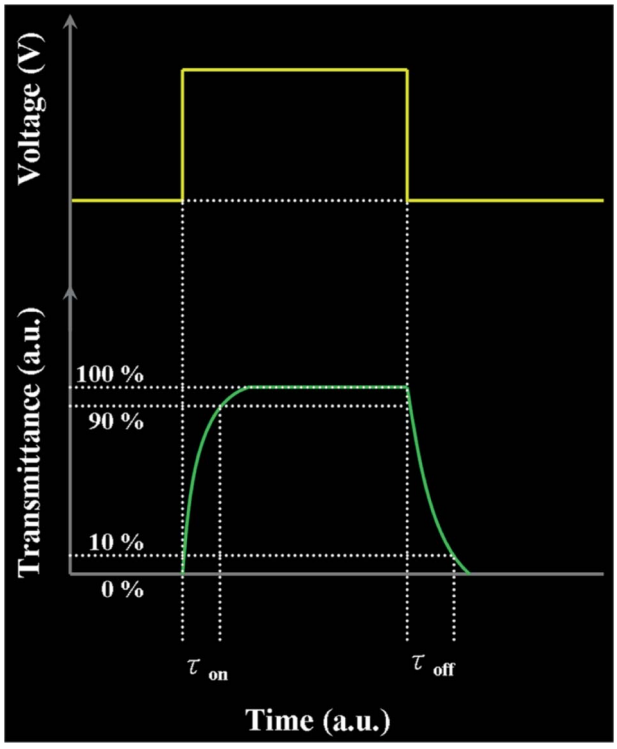

Figure 9. Definition of the rise time and fall time of the LC molecules (colour version online).

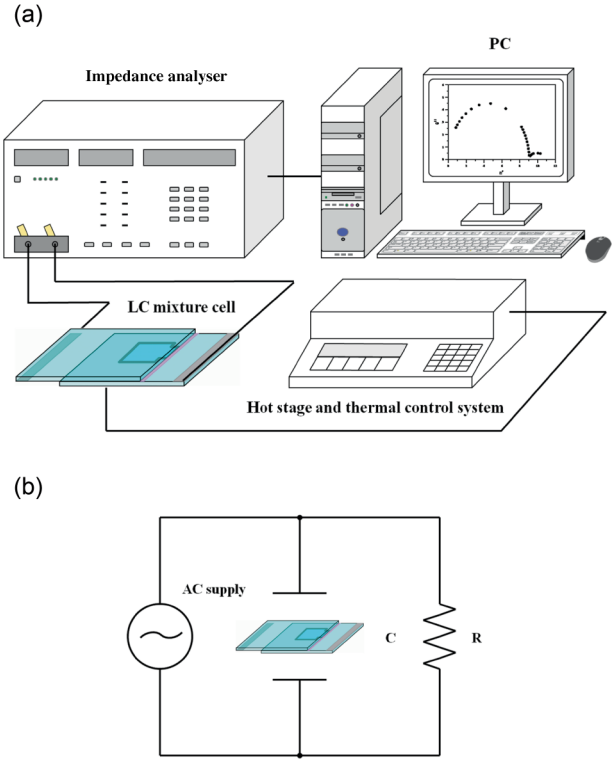

Figure 10. (a) Setup for measuring the dielectric behaviours of the LC mixture cells. (b) chart of the capacitor circuit (*R–C* circuit) (colour version online).

laser (10 mW, $\lambda = 632.8$ nm, Gondo Co., Ltd.) as the incident light source [48, 49], and placed the LC mixture cell between the crossed polarisers for measurement. By applying an alternating saturation voltage (10 Hz, square wave), the signal would be received and transformed by the photodiode (Electro-Optics Technology Co., Ltd., Models ET-2000) and displayed on the oscilloscope (Yokogawa Electric Co., Ltd., Models DL1200A). From the detected shapes of the waveform, we calculated the total response time, defined to be the sum of the rise time (τ_{on}) and fall time (τ_{off}).

$$\text{Total response time} = \tau_{on} + \tau_{off}. \quad (2)$$

Here, we defined the τ_{on} of the LC molecules to be the time required for the transmittance to rise from 10% to 90% as the dark state shifted to the bright state, and the τ_{off} to be the time required for the transmittance to fall from 90% to 10% as the bright state shifted to the dark state, as shown in Figure 9.

2.5.3 *Dielectric characteristics*

An impedance analyser (model Hewlett-Packard 4192A low frequency impedance analyser) was used to study the static dielectric permittivity of the sample in the frequency range 100 Hz to 13 MHz [167, 184–194] with an accuracy of 0.15% or better.

The dielectric measurements of the LC mixture cells were performed with a HP4192A (frequency range 10^2 Hz to 10^6 Hz; bias voltage 0.3 V ($V < V_{th}$) and 6 V ($V = V_{sat}$, saturation voltage of the mixture system) respectively) and a programmable temperature controller (Mettler FP-90 central process and FP-82HT hot stage; temperature measurement range 30–120°C). Figure 10(a) shows the setup for measuring the dielectric behaviour of the LC mixture cell. The principle of the measurement is to fill a cell essentially consisting of a pair of parallel electrode plates (ITO glass substrate) with the LC mixture solutions, which can be thought of as acting as a capacitor. We then connected it in parallel to the resistance to form an equivalent circuit (*R–C* circuit) as shown in Figure 10(b). From the figure, it can be seen that we used a fixed cell thickness of 4 μm. Before proceeding with the dielectric measurements, the LC mixture cells (which had already gone through the UV light irradiation process; CP ~89%) were heated by a hot stage to around 40°C above the materials' clear point (isotropic temperature). After maintaining the cells at constant temperature for 5 min (to form a homogeneous state), we slowly lowered the temperature of

the cells to room temperature so as to allow the LC molecules to settle into a more orderly arrangement before proceeding with the measurements as per our experimental procedures.

The dielectric constant (ε') and dielectric loss (ε'') of the LC mixture systems are given by [187, 189–194]

$$\varepsilon'(\text{real part}) = C_P \times d/\varepsilon_0 \times A, \tag{3}$$

$$\varepsilon'(\text{imaginary part}) = G_P/2\pi \times f \times C_0, \tag{4}$$

where C_P is the parallel connection capacitance (pF) of the LC mixture cell, d is the cell thickness (μm), ε_0 is the dielectric constant (8.854 pF m^{-1}) in vacuum, A is the parallel electrode area (m^2), G_P is the conductance (the reciprocal of the electrical resistance, siemens, S), f is the frequency (Hz) of the applied electrical field and C_0 is the capacitance (pF) of the empty cell.

3. Results and discussions

3.1 UV CP of the LC mixture systems

After the NLC and NSLC mixture solutions had been exposed to UV light irradiation for 0 to 30 min, PIPS led to the production of free radicals by the photo-initiator, leading to the former's interactions with the unsaturated functional groups (acetyl double bonds) of the photo-curable acrylic pre-polymer to produce co-polymerisation reactions. At this point, the solubility between the LC and photo-curable acrylic pre-polymer slowly dropped to the point where the reactions terminated and a complete phase separation was achieved. Under the influence of the photo-initiator, the unsaturated acetyl double bonds would be impacted, thereby causing the UV absorption values (Abs, λ_{max}) to fall and reach a saturation value. Therefore, we converted the changes in the UV absorption value of the NLC and NSLC mixture solutions (Figures 11(a) and 11(c)) during the period of UV light irradiation from 0 to 30 min to the UV CP (%) [48].

From the UV CP vs. UV light irradiation time graph (Figures 11(b) and 11(d)), it can be observed that the NSLC mixture system already reached a CP value of ~89% after 12 to 13 min of UV light irradiation (Figure 11 (d)); by contrast, it takes about 15 min to accomplish the same CP value in the NLC mixture system (Figure 11 (b)). From this phenomenon, we deduced that the system's rate of co-polymerisation reactions was faster than that of the NLC mixture system. However, after UV light irradiation for 30 min, the CP values of both of the NLC and NSLC mixture systems were all higher than ~97%.

The main reason we selected two LC mixture systems whose CP values were ~89% was to avoid the incomplete separation of the LC molecules from the copolymer volume of the photo-curable acrylic pre-polymer under insufficient UV light irradiation time, thereby leading to the PDLC film structure morphology. On the other hand, in the case when the UV light irradiation time was exceedingly long, although the phase separation process would be nearly complete, the cross-linking density of the polymer film would be larger and the degree of crystallisation would increase rapidly, resulting in the VACOF thus formed to be more brittle [48].

In order to achieve uniformity in the experimental conditions and avoid occurrence of the aforementioned scenarios, we therefore selected NLC and NSLC mixture systems with approximately the same CP values (~89%), for performing the relevant experiments.

3.2 Phase transition behaviours and POM observations of the LC mixture systems

We subjected the NLC and NSLC mixture compounds, which had already been processed by the UV light irradiation process (the CP values of both systems were ~89%, see Figure 11), to DSC thermal properties measurements and analysis, as well as POM (with cell thickness $d = 4$ μm) observations, with the results as shown in Figure 12 and Table 2.

As shown in Figure 12, the phase transition temperature of pure NLC does not vary significantly after the mixing of the photo-curable acrylic pre-polymer and photo-initiator (Table 2). In addition, the POM micro-photograph in the inset of Figure 12(a) revealed a nematic schlieren texture during the second cooling process (temperature ~30°C). On the other hand, the inset of Figure 12(b) shows that the nematic-type LC molecules of the NLC mixture system, after the photo-alignment process and being subjected to temperature conditions of under 30°C (second cooling), exhibited a uniform vertically aligned state and conoscopic pattern. Additionally, for the NSLC mixture system, our original intent was to mix a trace amount of pure SmA* LC (the POM picture in the inset of Figure 12(c) shows a uniform homeotropic texture and conoscopic pattern) into the NLC mixture system to enhance the vertical alignment effect in the original system. Nevertheless, what we found particularly intriguing during the experimental process was that the NSLC mixture system produced a special TGB phase (we tentatively named it the unknown TGB_{AX}^* phase). Further, in Figure 12(d) and Table 2, we can quite clearly see from the phase transition temperature curve during the DSC second cooling of the NSLC mixture compounds that, other than a slightly higher

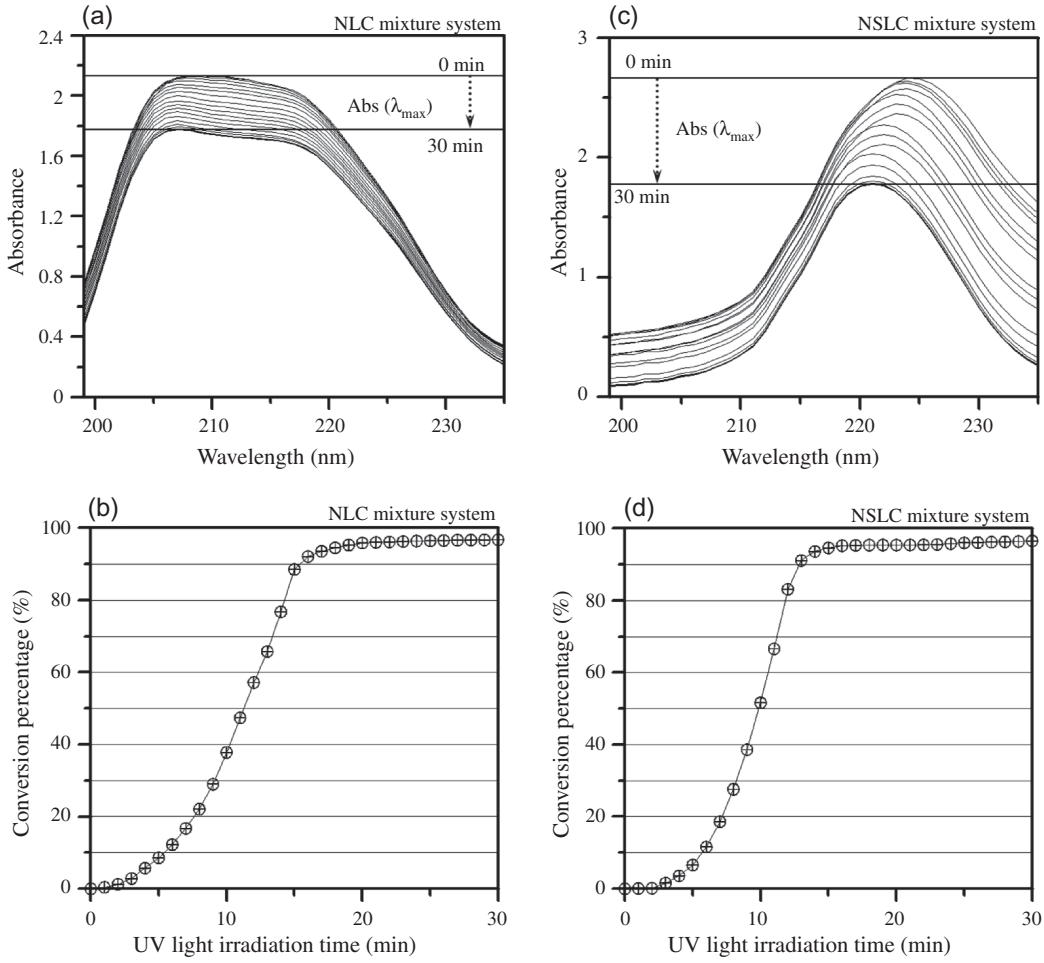

Figure 11. Variations in the UV absorption values ((a) and (c)) and UV CPs ((b) and (d)) of the NLC and NSLC mixture systems under UV light irradiation during the 0 to 30 min interval, respectively.

clear point than pure SmA* LC (caused by the disruption of the ordering of the SmA* type LC molecules by the nematic-type LC molecules), the most important result was that the temperature range of the TGB_{AX}* phase thus produced (as can be seen from the POM picture in the inset of Figure 12(d)) was rather broad (~40°C and it maintained the helix structure even after crystallisation, both under the second cooling process). It was also much closer to the room temperature condition, which holds the promise for increasing the application temperature range of the LC mixture materials. However, the TGB_{AX}* phase produced by this LC mixture system requires further experimental and theoretical studies for verification and determination of the exact cause of the optical texture (TGB_{AX}* phase), although it is our conjecture that the mixing of SmA* LC with high chirality was responsible for the emergence of the phase. It should be noted that since the CP values of the photo-curable acrylic prepolymer after UV light irradiation for both types of LC mixture system were ~89% and the melting points (T_m) were greater than 250°C, we only scanned within the LC phase transition temperature range during the DSC thermal analysis, and would thus not be able to observe the thermal transition behaviours of the acrylic copolymers.

3.3 Photo-alignment mechanism of the NSLC mixture system

In previous studies on photo-induced vertical alignment LC devices, POM and scanning electron microscopy (SEM, JEOL, JSM-6390LV) were utilised to prove that the copolymer structure morphology formed after the photo-alignment process was the VACOF with smooth surface, and not networked PDLC film (the devices operated in the scattering mode) [47–49]. The vertical alignment mechanism of the LC molecules were also described and studied in detail. In this experiment, one of the reasons we chose the SmA* LC with the terminal group alkyl carbon number of 10 was that the surface anchoring

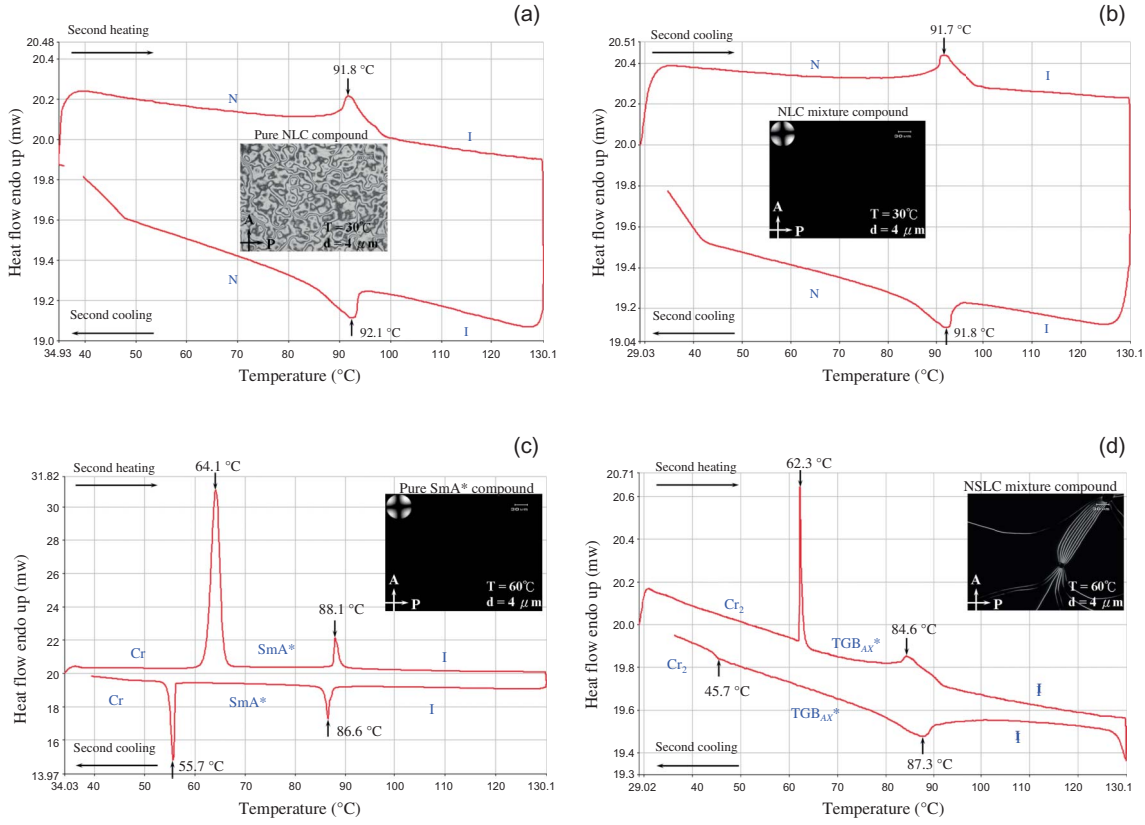

Figure 12. DSC traces obtained during two successive heating and cooling cycles for pure NLC and NLC mixtures ((a) and (b)) and pure SmA* and NSLC mixtures ((c) and (d)), respectively (Inset: Optical texture of all the mixtures during the second cooling, from POM observations and micro-photograph shots (with LC cell thickness $d = 4$ μm)).

Table 2. Phase transition temperature (°C) from the DSC thermograms and enthalpies (J g^{-1}) of transitions for all compounds.

	Phase transition temperature (°C)[a]								
Pure compounds	Cr	Heating (ΔH) Cooling (ΔH)	Cr	Heating (ΔH) Cooling (ΔH)	SmA*	Heating (ΔH) Cooling (ΔH)	N	Heating (ΔH) Cooling (ΔH)	I
Pure NLC	•	−20.0 (+27.2)[b]	×	–	×	–	•	91.8 (+ 2.2)	•
	•	−20.2 (−27.1)[c]	×	–	×	–	•	92.1 (−2.1)	•
Pure SmA*	×	–	•	64.1 (+55.0)	•	88.1 (+4.9)	×	–	•
	×	–	•	55.7 (−54.9)	•	86.6 (−4.8)	×	–	•
	Phase transition temperature (°C)[a]								
Mixture compounds	Cr_1	Heating (ΔH) Cooling (ΔH)	Cr_2	Heating (ΔH) Cooling (ΔH)	TGB_{AX}*	Heating (ΔH) Cooling (ΔH)	N	Heating (ΔH) Cooling (ΔH)	I
NLC mixture system	•	−20.5 (+33.7)	×	–	×	–	•	91.7 (+2.1)	•
	•	−20.7 (−33.3)	×	–	×	–	•	91.8 (−2.0)	•
NSLC mixture system	•	−23.3 (+65.7)	•	62.3 (+0.73)	•	84.6 (+1.14)	×	–	•
	•	−23.2 (−65.2)	•	45.7 (−0.71)	•	87.3 (−1.13)	×	–	•

Notes: [a] The phase transition temperatures were read at their maximum endothermic and exothermic peaks in the DSC thermograms obtained during the second heating and cooling cycles at 5°C min^{-1}.

[b, c] For the heating and cooling processes, we used positive (negative) values for endothermic (exothermic) variations in the enthalpies (ΔH). The acronyms are (applicable wherever used): Cr = crystalline phase; SmA* = chiral smectic A phase; N = nematic phase; TGB_{AX}* = twist grain boundary AX phase; I = isotropic liquid phase. (• = phase exists; × = phase does not exist; – = phase transition temperature and enthalpy variations do not exist.)

energy produced by the photo-alignment process was weaker [48, 109, 195, 196]. Therefore, we hoped to mix SmA* LC to increase the interaction forces (van der Waals forces) [47–49, 197–200] with the alkyl long carbon chain acrylic pre-polymer (also with an alkyl carbon number of 10) and also enhance the surface anchoring energy. Figure 4 illustrates the envisioned uniform distribution of the majority of the SmA* LC molecules onto the VACOF surface of the double layers after the photo-alignment process. However, under the POM with cross polarisers, we could clearly observe the special TGB_{AX}* phase (inset POM picture of Figure 12(d)) produced in the NSLC mixture system. We thus conjectured that not all of the SmA* LC molecules were uniformly distributed onto the VACOF surface of the double layers, and a trace fraction was dispersed among the NLC molecules, leading to the special helix arrangement structure which thereby produced the discontinuous domain optical texture. Nevertheless, due to the coexistence of the SmA* and nematic phase, the bright line filamentary texture observed under the POM might have arisen from the micro-defect caused by the slight rotation through an angle of one LC layer from another. In this case, the helix axis was perpendicular to the long axis of the LC molecules, and parallel to that of the smectic layer planes [148], with the LC molecules assuming a basic configuration structure as shown in Figure 1(a).

3.4 *Electro-optical studies of the LC mixture systems*

Figures 13(a) and 13(b) show the measured voltage-dependent transmittance of the NLC and NSLC mixture systems. In Figure 13 and Table 3, we can see clearly that although the NLC mixture system had a smaller threshold voltage (V_{th}) and driving voltage (V_{on}) in comparison to the NSLC mixture system, the mixing of SmA* LC had also tremendously improved the gray-scale switching performance of the LC device. In addition, the measured V_{th} and V_{on} for the NSLC mixture system were larger, which indirectly proved that the anchoring energy of the VACOF surface in this system was larger [195, 201].

The POM picture in the inset of Figure 13(a) indicated that, before a voltage was applied to the NLC mixture system, the LC molecules exhibited a uniform dark state. After the application of a voltage, all the LC molecules exhibited a single-domain bright state display with uniaxial orientation. The POM picture in the inset of Figure 13(b) also shows that before the application of a voltage ($V = 0$), there existed a special TGB_{AX}* phase. After the application of the saturation voltage ($V = V_{sat}$), we can see clearly that under the influence of the electrical

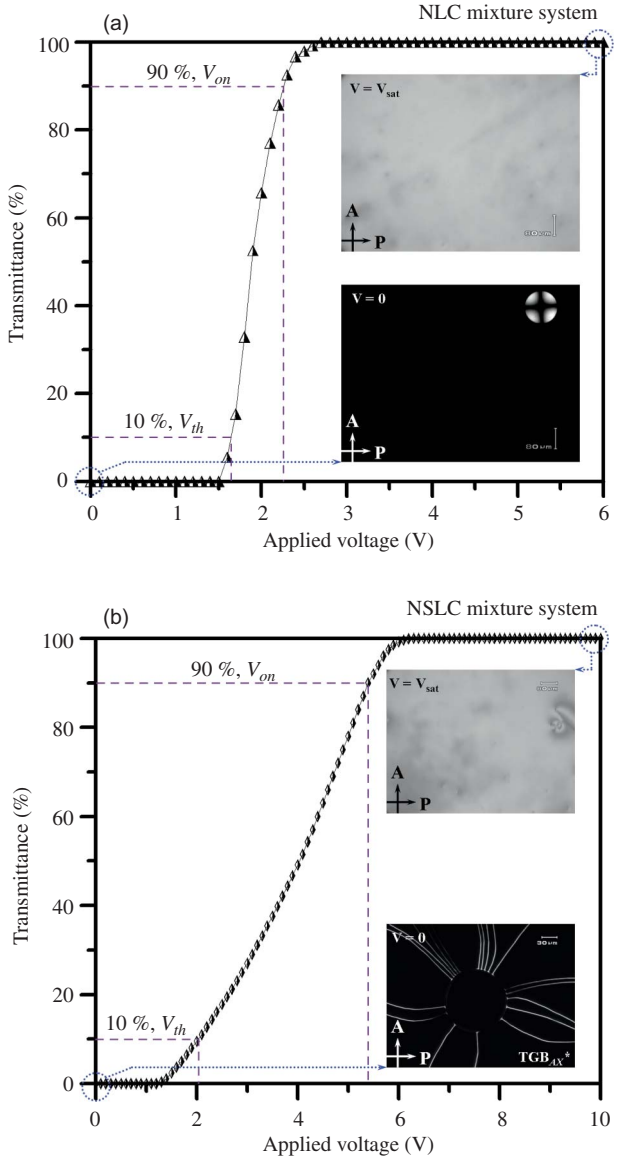

Figure 13. The transmittance vs. applied voltage relationship of the (a) NLC and (b) NSLC mixture systems (Inset: POM observations of the display conditions before and after a voltage was applied to the LC mixture cells).

Table 3. Threshold voltage (V_{th}), driving voltage (V_{on}), saturation voltage (V_{sat}) and contrast ratio (CR) of the LC mixture systems.

LC mixture system	V_{th} (V)	V_{on} (V)	V_{sat} (V)	Contrast ratio
NLC	1.64	2.27	6	1300:1
NSLC	2.02	5.41	10	-[a]

Note: [a] Since the special TGB_{AX}* phase in the NSLC mixture system was unknown, we did not measure and explore its CR value.

field all the LC molecules (including the trace fraction of SmA* LC) rotated in the direction of the electrical field, leading to the disintegration of the TGB_{AX}* phase and the appearance of the same single-domain bright state in the case of the NLC mixture system.

Furthermore, from Equation (5), one can calculate the theoretical value of V_{th} of the NLC used in the experiment to be ~2.22 V [196, 202]:

$$V_{th} = \pi\sqrt{K_{eff}/\varepsilon_0|-\Delta\varepsilon|}, \tag{5}$$

where V_{th} is the threshold voltage of the LC, K_{eff} is the effective elastic constant, ε_0 is the free space permittivity and $\Delta\varepsilon$ is the dielectric anisotropy of the LC. From Equation (5), we can see that V_{th} does not depend on the cell thickness. Additionally, from the empirical results of Table 3, we see that the V_{th} of the NLC and NSLC mixture systems were both smaller than the theoretical values in Equation (5), suggesting LC devices with fast driving [105, 195, 201, 203, 204]. Moreover, from Figures 13(a) and 13(b), it was also clear that both kinds of LC mixture cells maintained excellent bright state displays after the application of V_{sat}. From this, we conjectured that the LC mixture system also had a good voltage holding ratio (VHR), yet another important indicator of the vertical alignment characteristics of the LC molecules.

For the response time measurements of the LC mixture systems, the rise time (τ_{on}) and fall time (τ_{off}) can be calculated from the following equations [196, 202]:

$$\tau_{on} = \gamma_1 d^2/(\varepsilon_0|-\Delta\varepsilon|V^2 - K_{eff}\pi), \tag{6}$$

$$\tau_{off} = \gamma_1 d^2/K_{eff}\pi^2, \tag{7}$$

where η_1 is the rotation viscosity of the LC and V is the applied voltage. One can see from the response time measurements in Table 4 that τ_{off} was slightly larger than τ_{on}. The main reason for this was that the rise time is the time required for the LC molecules to generate electro-optical effects after being acted on by the electrical field, while the fall time is the time required for the LC molecules to be restored to their original locations on their own after removal of the electrical field. Therefore, Equation (7) does not involve the applied voltage. Thus, according to Equations (6) and (7), we can see that when using the same LC materials, the physical parameters of the LC itself aside, τ_{on} and τ_{off} are proportional to the square of the cell thickness d. Therefore, using a smaller cell thickness would increase the total response time of the LC cells. Although the viscosity and effective elastic constant of the material are also factors affecting the response time, they paled in comparison to the effect of the surface anchoring energy of the VACOF produced after the photo-alignment of the NLC and NSLC mixture systems on τ_{on} and τ_{off}. The experiment results are shown in Figure 14 and Table 4.

From the empirical data, it is clear that the mixing of a trace quantity of SmA* LC material into the NLC mixture system can dramatically improve the total response time. It is our belief that the improvement stemmed from the larger surface anchoring energy of the VACOF in the NSLC mixture system than that of the NLC mixture system. The total response times for both LC mixture systems ranged from 15 to 17 ms.

Table 4. Total response time measurements for the LC mixture systems.

LC mixture system	τ_{on} (ms)	τ_{off} (ms)	Total response time (ms)
NLC	8.21	8.50	16.71
NSLC	10.05	5.03	15.08

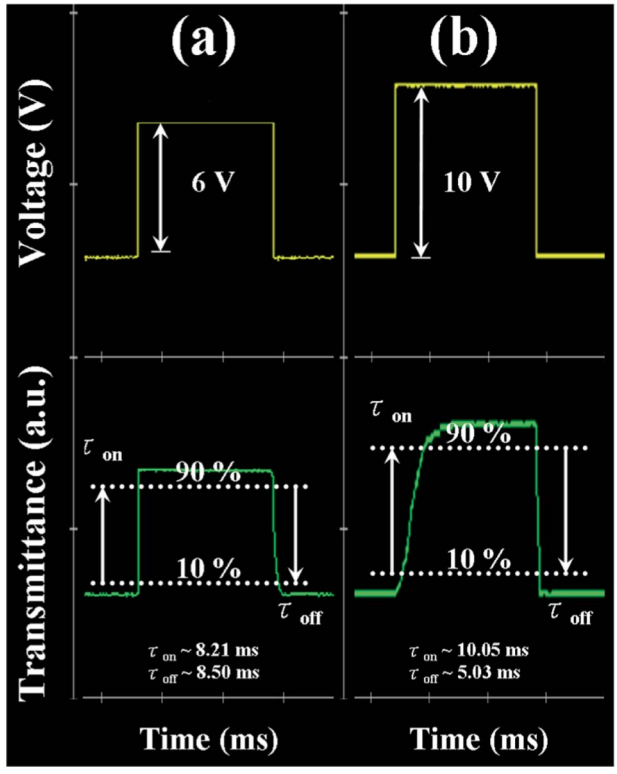

Figure 14. Measurements of the response time for the (a) NLC and (b) NSLC mixture systems (with cell thickness $d = 4$ μm) (colour version online).

3.5 *Preliminary dielectric behaviour studies of the LC mixture systems*

3.5.1 *Relationships of the dielectric constant and dielectric loss of the LC mixture systems with temperature*

From Figure 15(a), we see that when a miniscule voltage ($V < V_{th}$) was applied to the NLC mixture cell, the dielectric constant did not vary significantly with different frequencies. After the UV light irradiation process, almost all the LC molecules were in the vertically aligned state and when the applied voltage was smaller than the threshold voltage of the LC molecules, the dielectric characteristics of the material would not be affected. Furthermore, at high temperatures (when the temperature exceeded the clear point or isotropic temperature, T_{iso}, of the LC), the relatively low viscosity and high fluidity of the material meant that the thermal agitations of the molecules were so vigorous that the interactions between the dipoles dropped, resulting in changes in the dipole orientation and thus the molecule polarisation, leading to a decrease in the dielectric constant. Moreover, when the temperature dropped gradually from the clear point or isotropic temperature, T_{iso}, of the LC to under ~90°C, the dielectric constant at all frequencies rose rapidly. This was due to the fact that the LC mixture compound had undergone a phase transformation. Likewise, at high temperatures, the relatively low viscosity and mild thermal agitations of the molecules enabled the LC molecules to keep in step with variations in the electrical field at high frequencies, leading to rapid polarisation of the dipole and thus an increase in the dielectric constant. When the temperature dipped below ~70°C, the LC molecules slowly settled into a stable configuration, and the viscosity of the NLC mixture system increased at this point, while the dielectric constant dropped and stabilised.

Due to changes in the material's viscosity with temperature, the necessary time for polarisation also varied. Therefore, at a fixed frequency, the viscosity of the medium would be excessively high when the temperature was too low, and the polarisation process would

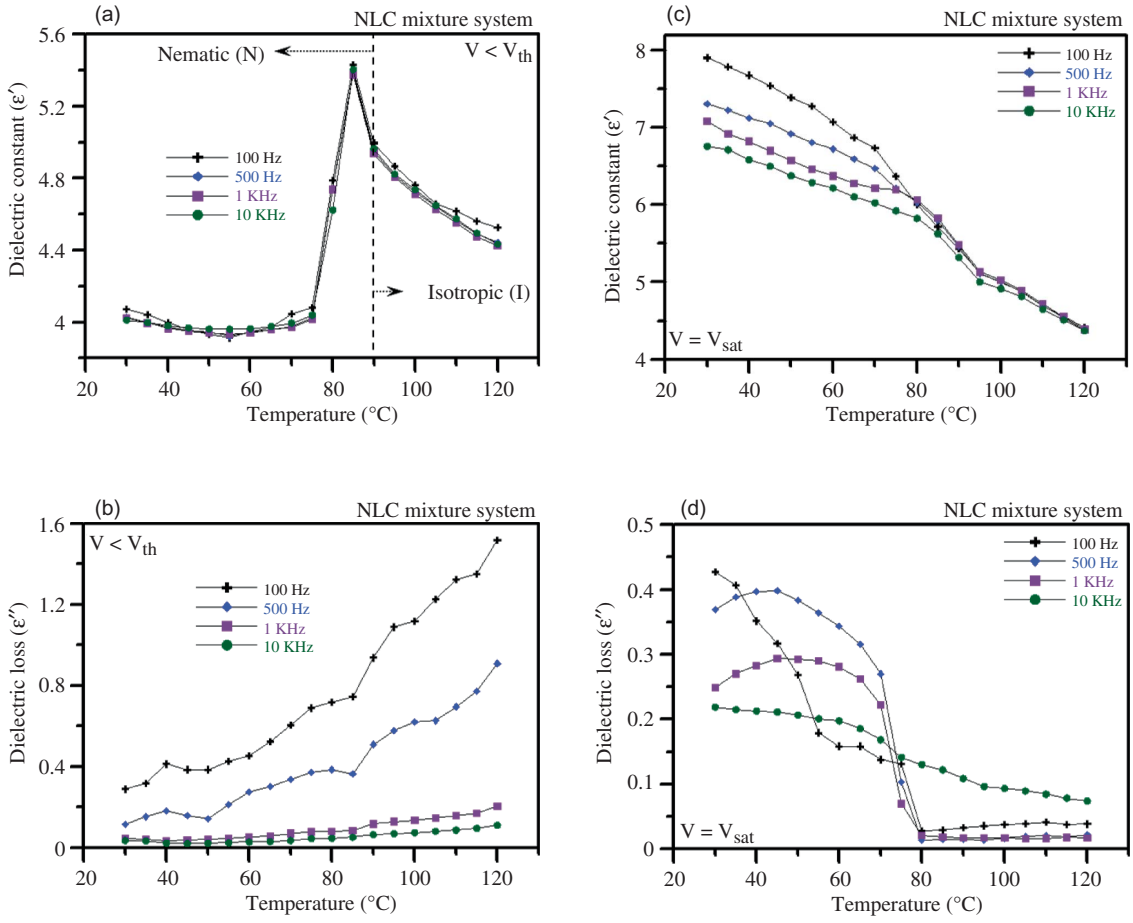

Figure 15. Relationships between the dielectric constant and temperature ((a) and (b)) as well as dielectric loss and temperature ((c) and (d)) before and after a voltage was applied to the NLC mixture system (colour version online).

be too slow. As such, the dipole orientation would not be able to keep up with the variations in the electrical field at this frequency, and the dielectric constant and dielectric loss would become comparatively small. This way, we can see clearly from Figure 15(b) that the dielectric loss would gradually drop with decrease in the temperature and increase in the frequency. When the temperature dropped gradually, the viscosity of the LC would increase and the molecules would be less thermally mobile and incapable of keeping up with the variations in the electrical field at high frequencies. Moreover, we could also learn about the relationship between the dielectric constant and temperature of the NLC mixture materials from the DSC thermal analyser picture or POM observation to indirectly infer the phase transition temperature behaviour (second cooling process) from the isotropic liquid phase to the nematic phase of the NLC mixture system.

Generally, when the external electrical field was increased, more dipoles would become aligned in the direction of the electrical field and the polarisation would increase. On the other hand, the conduction current flowing through the dielectric material is directly proportional to the voltage. Both scenarios would result in an increase of the dielectric loss. However, under the influence of the electrical field, in addition to the movements of the LC molecules being affected by the temperature, the dipole moments of the LC molecules would also be aligned in the direction of the electrical field. Therefore, both the dipole moments and the LC molecules were re-oriented. Figure 15(c) shows how, after the saturation voltage ($V = V_{sat}$) was applied to the NLC mixture cell, the external electrical field induced dipoles and subsequently a re-orientation in the polarisation, which increased the degree of polarisation (the permanent dipoles became polarised in the direction of the electrical field). Therefore, it can be seen that when the applied voltage was large, more dipoles would be induced and the orientation of the polarisation would occur faster, causing the dielectric constant to rise. However, with the increase in temperature, the thermal agitations of the molecules resulted in weaker interactions between the dipoles, and the dipole orientation became interrupted. Therefore, the dielectric constant would decrease with an increase in the temperature. Furthermore, the variations in the dielectric loss (Figure 15(d)) after the application of the saturation voltage were smaller in comparison with the case when $V < V_{th}$ (the application of a larger voltage led to more dipoles being induced and the LC molecules being more readily polarised). We were aware that our empirical data varied from what would normally be expected, namely that the dielectric loss of the NLC mixture system after the application of the saturation voltage was smaller. This is one area in which we hope to conduct further investigations to better understand the mechanism in play. The experimental results from Figures 16(a)–(d) were similar to those from Figures 15(a)–(d), other than the fact that the dielectric constant of the NLC mixture system with SmA* LC added exhibited an obvious increase. In addition, from Equations (5) and (6), we can see that an increase in the dielectric constant would imply a decrease in the threshold voltage (V_{th}) and an increase in the rise time (τ_{on}) of the LC device. Nonetheless, from our experimental data, we learned that while the mixing of SmA* LC did increase the dielectric constant, owing to the greater anchoring energy of the VACOF surface formed under the NSLC mixture system, a slight increase in V_{th} of the LC device resulted (although the τ_{off} did improve). Therefore, while the effect of the dielectric constant in Equations (5) and (6) is important, the anchoring energy of the alignment film surface is also a key consideration. As such, the CP of the LC mixture systems discussed in Section 3.1 would also be affected. This is due to the fact that, after the photo-alignment process, the PIPS caused by the UV light irradiation led to co-polymerisation reactions among the photocurable acrylic pre-polymer. Therefore, we understood that the CP of the system had yet to reach 100% (the CPs of both types of LC mixture systems used in the experiment were ~89%), and there would likely exist free radicals and acrylic pre-polymer from incomplete reactions that would roam free in the system and affect the dielectric behaviour. However, from our preliminary experimental findings, we knew that when there existed trace quantities of the ionic impurities in the system characteristics such as the dielectric properties, transmittance behaviour, response time, etc. of the LC mixture system would not be significantly affected.

3.5.2 Relationships of the dielectric constant and dielectric loss of the LC mixture systems with frequency

This subsection is devoted to the relationships between the measured dielectric constant and dielectric loss with frequency of the LC mixture systems at room temperature (~30°C). In accordance with the different polarisation mechanisms, the molecules can be classified into three categories based on the frequency: interfacial polarisation (Log F between 0 and 4), dipole polarisation (Log F between 5 and 9) and atom polarisation (Log F greater than 9).

From Figures 17(a) and 17(b), we see that when a miniscule voltage ($V < V_{th}$) was applied to the NLC and NSLC mixture systems, an obvious increase in the dielectric constant occurred after the mixing of SmA* LC. At room temperature, when the external

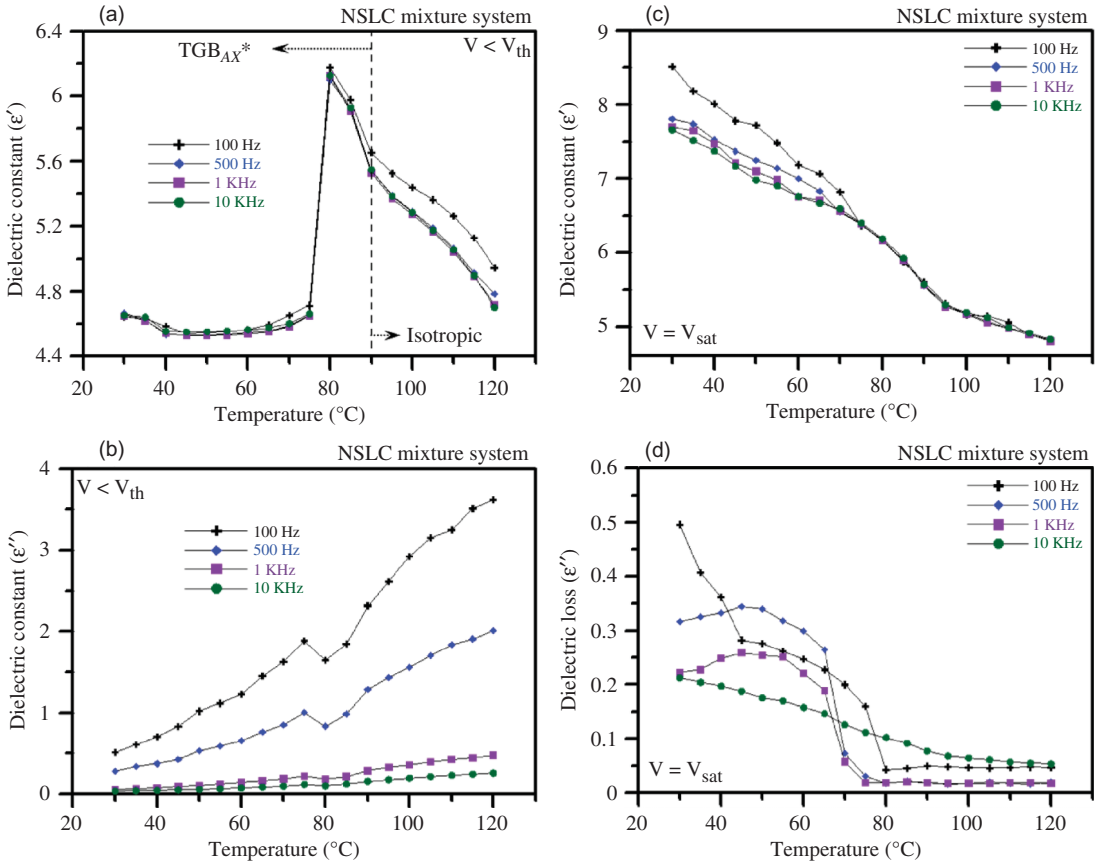

Figure 16. Relationships between the dielectric constant and temperature ((a) and (b)) as well as dielectric loss and temperature ((c) and (d)) before and after a voltage was applied to the NSLC mixture system (colour version online).

applied voltage is very small, all the LC molecules will exhibit a stable, vertically aligned state, resulting in an almost constant initial dielectric constant. Additionally, with the increase of the frequency (we also need to take into consideration the viscosity of the dielectric material), the orientation of the dipoles within the dielectric material would become affected by frictional resistance and start lagging behind the variations in the electrical field. Therefore, electrical energy would be absorbed (dielectric absorption), leading to forced vibrations and thus energy dissipation (dielectric relaxation phenomena). At this point, the material would heat up, resulting in further increases in the dielectric loss to a maximum. On the other hand, Figures 18(a) and 18(b) demonstrate the conditions after a saturated voltage ($V = V_{sat}$) was applied to the NLC and NSLC mixture systems. With the application of a large electrical field, dipoles are easily induced among the LC molecules by the external electrical field, resulting in an increase in the dielectric constant. In contrast, the dielectric loss will also increase gradually. This experiment was performed at room temperature, but an increase in the temperature and thus thermal agitations would help the LC molecules keep up with the variations in the electrical field at high frequencies and thus reduce dielectric loss. We performed our experiment at commonly used application temperatures.

3.5.3 *Cole–Cole plots for the LC mixture systems*

As can be seen from Figure 19, the Cole–Cole plots (ε″ versus ε′) for the NLC and NSLC mixture systems both increased with increasing applied voltage and shifted right. This phenomenon illustrated that an increased voltage led to higher dielectric absorption at low frequencies. However, as the frequency increased, the dielectric absorption dropped. This was due to the fact that the LC molecules were becoming less capable of keeping up with the variations in the electrical field at high frequencies. Likewise, greater dielectric absorption meant greater dielectric loss. At this point, the dielectric relaxation phenomenon would occur, and from the Cole–Cole plots in Figures 19(a) and 19(b), one can see quite clearly that both kinds of LC mixture systems at the saturation voltage would exhibit larger dielectric absorption and thus shift to the right.

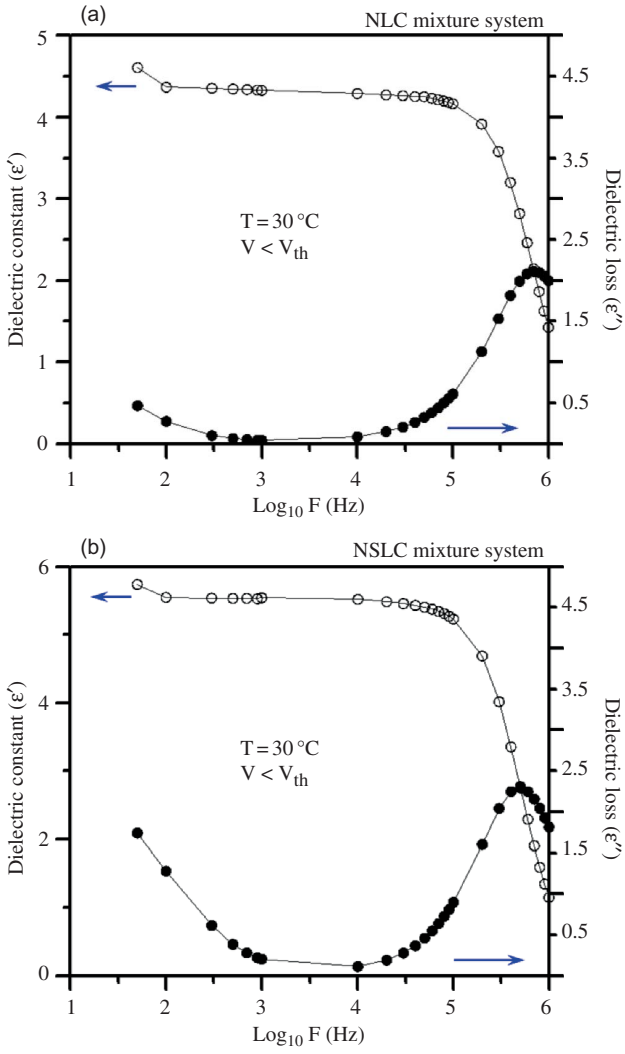

Figure 17. Typical experimental dielectric spectra (relative dielectric constant and loss) in the frequency range 50 Hz–1 MHz acquired in the (a) NLC and (b) NSLC mixture systems (0.3 V, $V > V_{th}$) at room temperature (~30°C).

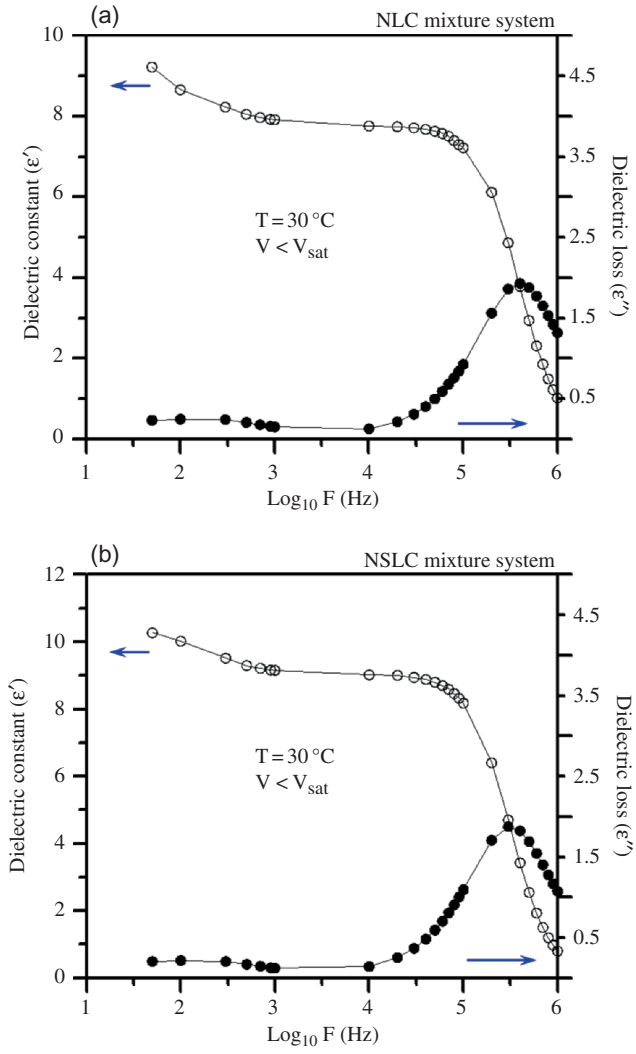

Figure 18. Typical experimental dielectric spectra (relative dielectric constant and loss) in the frequency range 50 Hz–1 MHz acquired in the (a) NLC and (b) NSLC mixture systems (6 V, $V = V_{sat}$) at room temperature (~30°C).

4. Conclusions

In summary, utilising previously demonstrated non-contact mode photo-alignment techniques, we successfully fabricated LC devices with vertically aligned effect pseudo-PI VACOF. In this study, we further mixed two SmA* phase LCs we had newly synthesised into a NLC mixture system with the photo-induced vertical alignment effect. The pure SmA* LC molecules exhibited a dark state with homeotropic aligned optical texture under POM with cross polarisers, and we therefore mixed a trace amount of SmA* LC into the original NLC mixture system to promote vertical alignment among the LC molecules. However, during the experiment, we discovered a special, unknown optical texture (a twist grain boundary AX phase, TGB_{AX}* phase) in the NSLC mixture system, which greatly intrigued us and captured our imagination. The mixing of SmA* LC in the NLC mixture system not only enhanced the anchoring energy and dielectric properties of the VACOF surface, but also improved the gray-scale switching and response time.

In the future, due to the fact that the TGB phases produced from normal LC mixture systems all occurred in liquid crystalline materials with SmA* and N* phases, we look forward to further investigating the formation, characteristics and applications of the TGB_{AX}* phase (SmA* and nematic-type LC mixture system). After measurement and analysis of the electro-optical properties of the LC mixture systems, we are confident that the use of the non-contact photo-polymerisation method in conjunction

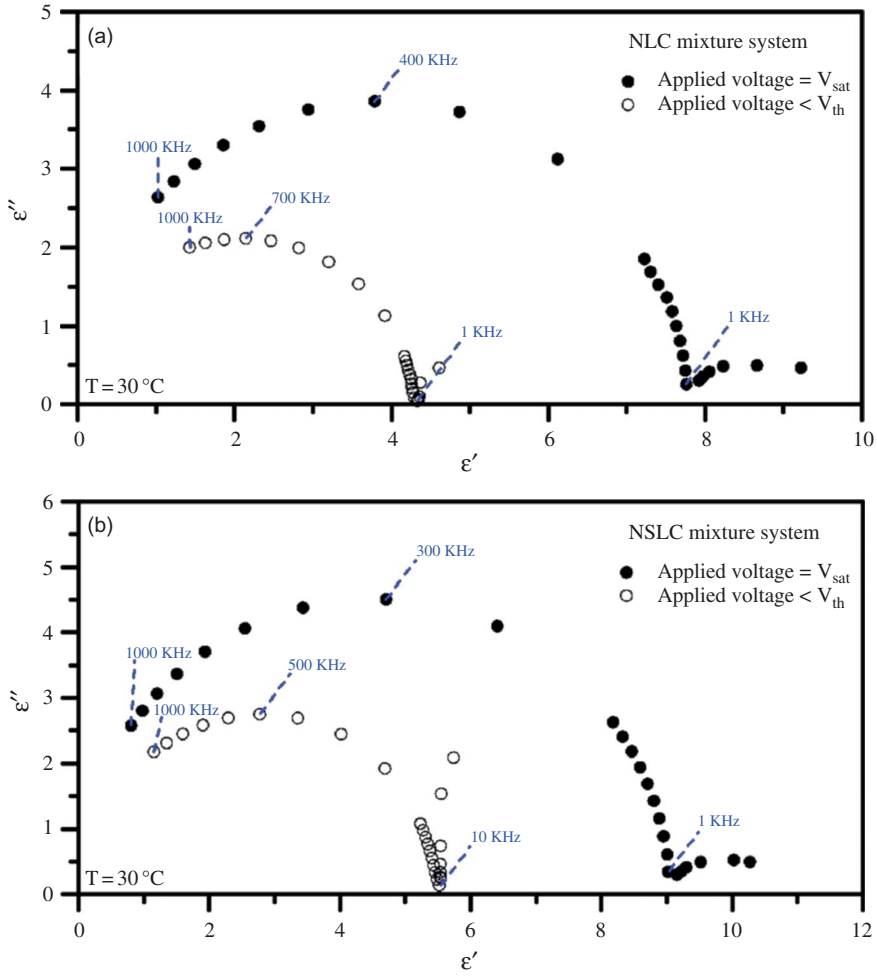

Figure 19. Cole–Cole plots of the NLC and NSLC mixture systems at room temperature (~30°C).

with flexible plastic substrate, multi-domain vertical alignment (MVA) technology, etc. holds great promise for fabricating LC devices with wide viewing angle and high contrast ratio characteristics. Moreover, we will also continue to study in-depth this unique NSLC mixture system, and hope to make further contributions to the LCD industry.

Acknowledgements

The authors would like to thank Mr Kai-Neng Yang from Chimei Innolux Corporation for supplying the photo-curable acrylic pre-polymer and photo-initiator materials for the experiment, and for offering numerous advice and suggestions which were invaluable in facilitating the smooth completion of the experiment.

References

[1] Haaren, J.V. *Nature (London, UK)* **2001**, *411*, 29–30.
[2] Sugiyama, T.; Kuniyasu, S.; Seo, D.S.; Fukuro, H.; Kobayashi, S. *Jpn. J. Appl. Phys.* **1990**, *29*, 2045–2051.
[3] Egerton, P.L.; Pitts, E.; Reister, A. *Macromolec.* **1981**, *14*, 95–100.
[4] Castellano, J.A. *Mol. Cryst. Liq. Cryst.* **1983**, *94*, 33–41.
[5] Geary, J.M.; Goodby, J.W.; Kmetz, A.R.; Patel, J.S. *J. Appl. Phys.* **1987**, *62*, 4100–4187.
[6] Ichimura, K.; Suzuki, Y.; Seki, T.; Hosoki, A.; Aoki, K. *Langmuir* **1988**, *4*, 1214–1216.
[7] Gibbons, W.M.; Shannon, P.J.; Sun, S.T.; Swetlin, B.J. *Nature (London, UK)* **1991**, *351*, 49–50.
[8] Schadt, M.; Schmitt, K.; Kozinkov, V.; Chigrinovl, V. *Jpn. J. Appl. Phys.* **1992**, *31*, 2155–2164.
[9] Nishikawa, M.; Yokoyama, Y.; Bessho, N.; Seo, D.S.; Iimura, Y.; Kobayashi, S. *Jpn. J. Appl. Phys.* **1994**, *33*, L810–L812.
[10] Shannon, P.J.; Gibbons, W.M. *Nature (London, UK)* **1994**, *368*, 532–533.
[11] Ichimura, K.; Akita, Y.; Akiyama, H.; Hayashi, Y.; Kudo, K. *Jpn. J. Appl. Phys.* **1996**, *35*, L992–L995.
[12] Schadt, M.; Seiberle, H.; Schuster, A. *Nature (London, UK)* **1996**, *381*, 212–215.
[13] Lee, K.W.; Lien, A.; Stathis, J.H.; Paek, S.H. *Jpn. J. Appl. Phys.* **1997**, *36*, 3591–3597.
[14] Wang, Y.; Xu, C.; Kanazawa, A.; Shiono, T.; Ikeda, T. *J. Appl. Phys.* **1998**, *84*, 181–188.

[15] Wang, Y.; Xu, C.; Kanazawa, A.; Shiono, T.; Ikeda, T. *J. Appl. Phys.* **1998**, *84*, 4573–4578.
[16] Wang, Y.; Kanazawa, A.; Shiono, T.; Ikeda, T. *Appl. Phys. Lett.* **1998**, *72*, 545–1–545–3.
[17] Nishikawa, M.; West, J.L. *Jpn. J. Appl. Phys. Part 1* **1999**, *38*, 5183–5188.
[18] Han, K.J.; Jung, Y.; Choi, H.H.; Hwang, H.K.; Lee, S.; Humjang, S. *J. Appl. Phys.* **1999**, *86,* 1854–1859.
[19] Perny, S.; Barny, P.L.; Delaire, J. *Liq. Cryst.* **2000**, *27*, 349–358.
[20] Ichimura, K. *Chem. Rev.* **2000**, *100*, 1847–1874.
[21] Contoret, A.E.A.; Farrar, S.R.; Jackson, P.O.; Khan, S.M.; May, L.; O'Neill, M.; Nicholls, J.E.; Kelly, S.M.; Richards, G.J. *Adv. Mater. (Weinheim, Ger.)* **2000**, *12*, 971–974.
[22] Wang, Y.; Xu, S.; Kanazawa, A.; Shiono, T.; Ikeda, T.; Matsuki, Y.; Takeuchi, U. *Liq. Cryst.* **2001**, *28*, 473–475.
[23] Fang, Y.J.; Chen, S.M.; Shashidhar, R. *Langmuir* **2001**, *17*, 1549–1551.
[24] Lee, B.; Clark, N.A. *Science* **2001**, *291*, 2576–2580.
[25] Stöhr, J.; Samant, M.G.; Lüning, J.; Callegari, A.C.; Chaudhari, P.; Doyle, J.P.; Lacey, J.A.; Lien, S.C.A.; Purushothaman, S; Speidell, J.L. *Science* **2001**, *292*, 2299–2302.
[26] Choi, D.H.; Cha, Y.K. *Bull. Kor. Chem. Soc.* **2001**, *23*, 587–592.
[27] Behdani, M; Keshmiri, H.S.; Soria, S; Bader, A.M.; Ihlemann, J; Marowsky, G.; Rasing, T. *Appl. Phys. Lett.* **2003**, *82*, 2553–1–2553–3.
[28] Huang, D.D.; Pozhidaevl, E.P.; Chigrinov, V.G.; Cheung, H.L.; Ho, Y.L.; Kwok, H.S. *Displays* **2004**, *25*, 21–29.
[29] Parka, J.H.; Khoo, I.C.; Yu, C.J.; Jung, M.S.; Lee, S.D. *Appl. Phys. Lett.* **2005**, *86,* 021906–1–021906–3.
[30] Paterson, M.J. *Diam. Relat. Mater.* **1996**, *5*, 1407–1413.
[31] Paterson, M.J. *Diam. Relat. Mater.* **1998**, *7*, 908–915.
[32] Chaudhari, P.; Lacey, J.A.; Lien, S.C.A.; Speidell, J.L. *Jpn. J. Appl. Phys.* **1998**, *37*, L55–L56.
[33] Chaudhari, P.; Lacey, J.; Doyle, J.; Galligan, E.; Lien, S.C.A.; Callegari, A.; Hougham, G.; Lang, D.N.; Andry, S.P.; John, R.; Yang, H.K.; Lu, M.; Cai, C.; Speidell, J.; Purushothaman, S.; Ritsko, J.; Samant, M.; Stöhr, J.; Nakagawa, Y.; Katoh, Y.; Saitoh, Y.; Sakai, K.; Satoh, H.; Odahara, S.; Nakano, H.; Nakagaki, J.; Shiota, Y. *Nature (London, UK)* **2001**, *411*, 56–59.
[34] Gwag, J.S.; Park, K.H.; Kang, D.J.; Jhun, C.G.; Kim, H.; Cho, S.J.; Yoon, T.H.; Kim, J.C. *Jpn. J. Appl. Phys.* **2003**, *42*, L468–L471.
[35] Lu, X.M.; Lu, Q.H.; Zhu, Z.K.; Yin, J.; Wang, Z.G. *Chem. Phys. Lett.* **2003**, *377*, 433–438.
[36] Saunders, F.C.; Staromlynska, J.; Smith, G.W.; Daniel, M.F. *Mol. Cryst. Liq. Cryst.* **1985**, *122*, 297–308.
[37] Gupta, R.K.; Suresh, K.A.; Guo, R.; Kumar, S. *Anal. Chim. Acta.* **2006**, *568*, 109–118.
[38] Zhurin, V.V.; Kaufman, H.R.; Robinson, R.S. *Plasma Sources Sci. Technol.* **1999**, *8*, R1–R20.
[39] Newsome, C.J.; O'Neill, M. *J. Appl. Phys.* **2002**, *92*, 1752–1756.
[40] Yaroshchuk, O.; Kravchuk, R.; Dobrovolskyy, A.; Qiu, L.; Lavrentovich, O.D. *Liq. Cryst.* **2004**, *31*, 859–869.
[41] Chou, S.Y.; Krauss, P.R.; Renstrom, P.J. *Science* **1996**, *272*, 85–87.
[42] Xia, Y.; Whitesides, G.M. *Angew. Chem. Int. Ed.* **1998**, *37*, 551–575.
[43] Marzolin, C.; Smith, S.P. Prentiss, M.; Whitesides, G.M. *Adv. Mater. (Weinheim, Ger.)* **1998**, *10*, 571–574.
[44] Chou, S.Y.; Keimei, C.; Gu, J. *Nature (London, UK)* **2002**, *417*, 835–837.
[45] Chiou, D.R.; Yeh, K.Y.; Chen, L.J. *Appl. Phys. Lett.* **2006**, *88*, 133123–1–133123–3.
[46] Chiou, D.R.; Chen, L.J. *Langmuir* **2006**, *22*, 9403–9408.
[47] Lin, F.H.; Ho, C.Y.; Lee, J.Y. *J. Technol.* **2011**, in press.
[48] Ho, C.Y.; Lee, J.Y. *Liq. Cryst.* **2010**, *37*, 997–1012.
[49] Tsai, P.S.; Ho, C.Y.; Lee, J.Y. *J. Technol.* **2011**, in press.
[50] Vorflusev, V.; Kumar, S. *Science* **1999**, *283*, 1903–1905.
[51] Vorflusev, V.; Kim, J.H.; Kumar, S. *Pramana-J. Phys.* **1999**, *53*, 121–129.
[52] Acharya, B.R.; Kim, J.H.; Kumar, S. *Jpn. J. Appl. Phys. Part 2* **1999**, *38*, L1538–L1540.
[53] Qian, T.; Kim, J.H.; Kumar, S.; Taylor, P.L. *Phys. Rev. E: Stat., Nonlinear, Soft Matter Phys.* **2000**, *61*, 4007–4010.
[54] Reznikov, Y.; Ostroverkhova, O.; Singer, K.D.; Kim, J.H.; Kumar, S.; Lavrentovich, O.; Wang, B.; West, J.L. *Phys. Rev. Lett.* **2000**, *84*, 1930–1–1930–4.
[55] Kim, I.; Kim, J.H.; Kang, D.; Kooijman, D.M.A.; Kumar, S. *J. Appl. Phys.* **2002**, *92*, 7699–7701.
[56] Wang, Q.; Chien, L.C.; Kumar, S. *Appl. Phys. Lett.* **2003**, *83*, 3698–1–3698–3.
[57] Kim, J.H.; Kumar, S. *Jpn. J. Appl. Phys.* **2004**, *43*, 7050–7053.
[58] Kim, J.H.; Vorflusev, V.; Kumar, S. *Displays* **2004**, *25*, 207–213.
[59] Kim, J.H.; Kumar, S. *J. Lightwave Technol.* **2005**, *23*, 628–632.
[60] Wang, Q.; Park, J.O.; Srinivasarao, M.; Qiu, L.; Kumar, S. *Jpn. J. Appl. Phys.* **2005**, *44*, 3115–3120.
[61] Wang, Q.; Kumar, S. *Appl. Phys. Lett.* **2005**, *86*, 071119–1–071119–3.
[62] Kumar, S.; Kim, J.H.; Shi, Y. *Phys. Rev. Lett.* **2005**, *94*, 077803–1–077803–4.
[63] Wang, Q.; Guo, R.; Kumar, S. *J. Soc. Inf. Display* **2006**, *14*, 545–561.
[64] Wang, Q.; Guo, R.; Daj, M.R.; Kang, S.W.; Kumar, S. *Jpn. J. Appl. Phys.* **2007**, *46*, 299–303.
[65] Choi, H.; Kim, D.W.; Rhie, K.W.; Hong, M.P.; Shin, S.T.; Kumar, S.; Jang, W.G.; Lee, B.W.; Kim, K.H. *Jpn. J. Appl. Phys.* **2008**, *47*, 1008–1011.
[66] Stannarius, R.; Crawford, G.P.; Chien, L.C.; Doane, J.W. *J. Appl. Phys.* **1991**, *70*, 135–143.
[67] Chidichimo, G.; Arabia, G.; Doane, J.W.; Golemme, A. *Liq. Cryst.* **1989**, *131*, 1443–1452.
[68] Fan, Y.H.; Ren, H.; Wu, S.T. *Opt. Express* **2003**, *11*, 3080–3086.
[69] Fan, Y.H.; Lin, Y.H.; Ren, H.; Gauza, S.; Wu, S.T. *Appl. Phys. Lett.* **2004**, *84*, 1233–1–1223–3.
[70] Fan, Y.H.; Ren, H.; Liang, X.; Lin, Y.H.; Wu, S.T. *Appl. Phys. Lett.* **2004**, *85*, 2451–1–2451–3.
[71] Choi, S.W.; Matsumoto, S.; Takanishi, Y.; Ishikawa, K.; Nishiyama, I.; Kawamura, J.; Takada, H.; Takezoe, H. *Org. Electron.* **2006**, *7*, 295–299.
[72] Doane, J.W.; Vaz, N.A.; Wu, B.G.; Zumer, S. *Appl. Phys. Lett.* **1986**, *48*, 26–9–1–269–3.

[73] Shimada, E.; Uchida, T. *Jpn. J. Appl. Phys.* **1992**, *31*, L352–L354.
[74] Takatsu, H.; Takeuchi, K.; Umezu, Y. *Mol. Cryst. Liq. Cryst.* **1993**, *225*, 81–88.
[75] Noh, C.H.; Jung, J.E.; Kim, J.Y.; Sakong, D.S.; Choi, K.S. *Mol. Cryst. Liq. Cryst.* **1993**, *237*, 299–309.
[76] Smith, G.W. *Mol. Cryst. Liq. Cryst.* **1994**, *241*, 77–89.
[77] Craighead, H.G.; Cheng, J.; Hackwood, S. *Appl. Phys. Lett.* **1982**, *40*, 22–1–22–3.
[78] Drzaic, P.S. *J. Appl. Phys.* **1986**, *60*, 2142–2148.
[79] Vaz, N.A.; Smith, G.W.; Montgomery, G.P. Jr. *Mol. Cryst. Liq. Cryst.* **1987**, *146*, 1–16.
[80] Vaz, N.A.; Smith, G.W.; Montgomery, G.P. Jr. *Mol. Cryst. Liq. Cryst.* **1987**, *146*, 17–34.
[81] Vaz, N.A.; Montgomery, G.P. Jr. *J. Appl. Phys.* **1987**, *62*, 3161–3172.
[82] West, J.L. *Mol. Cryst. Liq. Cryst.* **1988**, *157*, 427–441.
[83] Doane, J.W.; Golemme, A.; West, J.L.; Whitehead, J.B. Jr.; Wu, B.G. *Mol. Cryst. Liq. Cryst.* **1988**, *165*, 511–532.
[84] Smith, G.W. *Mol. Cryst. Liq. Cryst.* **1991**, *196*, 89–102.
[85] Yamaguchi, R.; Sato, S. *Jpn. J. Appl. Phys.* **1991**, *30*, L616–L618.
[86] Jiang, P.; Asada, T. *Mol. Cryst. Liq. Cryst.* **1992**, *222*, 87–96.
[87] Radianguenebalid, M.; Sixou, P. *Mol. Cryst. Liq. Cryst.* **1992**, *220*, 53–62.
[88] Nolan, P.; Tillin, M.; Coates, D. *Liq. Cryst.* **1993**, *14*, 339–344.
[89] Takiazawa, K.; Kikuchi, J.; Fujikake, H.; Narnkawa, Y.; Tada, K. *Jpn. J. Appl. Phys.* **1994**, *33*, 1346–1351.
[90] Lovinger, A.J.; Amundson, K.R.; Davis, D.D. *Chem. Mater.* **1994**, *6*, 1726–1736.
[91] Fung, Y.K.; Yang, D.K.; Ying, S.; Chien, L.C.; Zumer, S.; Doane, J.W. *Liq. Cryst.* **1995**, *19*, 797–801.
[92] Kato, K.; Tanaka, K.; Tsuru, S.; Sakai, S. *Jpn. J. Appl. Phys. Part 1* **1995**, *34*, 554–559.
[93] Tondiglia, V.P.; Natarajan, L.V.; Sutherland, R.L. *Opt. Lett.* **1995**, *20*, 1325–1327.
[94] Rajaram, C.V.; Hudson, S.D.; Chien, L.C. *Chem. Mater.* **1995**, *7*, 2300–2308.
[95] Rajaram, C.V.; Hudson, S.D.; Chien, L.C. *Chem. Mater.* **1996**, *8*, 2451–2460.
[96] Cheng, S.X.; Bai, R.K.; Zou, Y.F.; Pan, C.Y. *J. Appl. Phys.* **1996**, *80*, 1991–1995.
[97] Drzaic, P.S. *Liquid Crystal Dispersions*; World Scientific: Singapore, 1995.
[98] Crawford, G.P.; Zumer, S. *Liquid Crystals in Complex Geometries*; Taylor and Francis: London, 1996.
[99] Chung, D.B.; Tsuda, H.; Chida, H.; Mochizuki, A. *Mol. Cryst. Liq. Cryst.* **1997**, *304*, 81–87.
[100] Liu, J.H.; Liu, H.S.; Tsai, F.R. *Polym. Int.* **1997**, *42*, 385–392.
[101] Legrange, J.D.; Carter, S.A.; Fuentes, M.; Boo, J.; Freeny, A.E.; Cleveland, W.; Miller, T.M. *J. Appl. Phys.* **1997**, *81*, 5984–5991.
[102] Carter, S.A.; Legrange, J.D.; White, W.; Boo, J.; Wiltzius, P. *J. Appl. Phys.* **1997**, *81*, 5992–5999.
[103] Tondiglia, V.P.; Natarajan, L.V.; Neal, R.M.; Sutherland, R.L.; Bunningts, T.J. *Mater. Res. Soc. Symp. Proc.* **1997**, *479*, 235–240.
[104] Takizawa, K.; Fujii, T.; Kawakita, M.; Kikuchi, H.; Fujikake, H.; Yokozawa, M.; Murata, A.; Kishi, K. *Appl. Optics* **1997**, *36*, 5732–5747.
[105] Nwphew, J.B.; Nihei, T.C.; Carter, S.A. *Phys. Rev. Lett.* **1998**, *80*, 3276–3279.
[106] Nastal, E.; Zuranska, E.; Mucha, M. *J. Appl. Polym. Sci.* **1999**, *71*, 455–463.
[107] Patnaik, S.S.; Pachter, R. *Polym.* **1999**, *40*, 6507–6519.
[108] Bhargava, R.; Wang, S.Q.; Koenig, J.L. *Macromolec.* **1999**, *32*, 8989–8995.
[109] Prk, N.H.; Cho, S.A.; Kim, J.Y.; Suh, K.D. *J. Appl. Polym. Sci.* **2000**, *77*, 3178–3188.
[110] Whitehead J.B. Jr.; Crawford, G.P. *Polym. Prepr.* **2000**, *41*, 1066–1067.
[111] Dierking, I. *Adv. Mater. (Weinheim, Ger.)* **2000**, *12*, 167–181.
[112] Nicoletta, F.P.; Lanzo, J.; Filpo, G.D.; Chidichimo, G. *Langmuir* **2001**, *17*, 534–536.
[113] Du, F.; Wu, S.T. *Appl. Phys. Lett.* **2003**, *83*, 1310–1–1310–3.
[114] Chen, T.J.; Chen, Y.F.; Sun, C.H.; Wu, J.J. *Jpn. J. Appl. Phys.* **2004**, *43*, L557–L559.
[115] Gelinck, G.H.; Huitema, H.E.A.; Veenendaal, E.V.; Cantatore, E.; Schrijnemakers, L.; Putten, J.B.P.H.V.D.; Geuns, T.C.T.; Beenhakkers, M.; Giesbers, J.B.; Huisman, B.H.; Meijer, E.J.; Benito, E.M.; Touwslager, F.J.; Marsman, A.W.; Rens, B.J.E.V.; Leeuw, D.M.D. *Nat. Mater.* **2004**, *3*, 106–110.
[116] Kihara, H.; Miura, T.; Kishi, R.; Kaito, A. *Polym.* **2004**, *45*, 6357–6363.
[117] Kihara, H.; Miura, T. *Polym.* **2004**, *46*, 10378–10382.
[118] Buyuktanir, E.A.; Mitrokhin, M.; Holter, B.; Glushchenko, A.; West, J.L. *Jpn. J. Appl. Phys.* **2006**, *45*, 4146–4151.
[119] Blinov, L.; Chigrinov, V. *Electrooptical Effects in Liquid Crystal*; Springer: Berlin, 1993.
[120] Hikmet, R.A.M. *J. Appl. Phys.* **1990**, *68*, 4406–4412.
[121] Krongauz, V.V.; Schmelzer, E.R.; Yohannan, R.M. *Polym.* **1991**, *32*, 1654–1662.
[122] Hikmet, R.A.M.; Boots, H.M.J. *Phys. Rev. E: Stat., Nonlinear, Soft Matter Phys.* **1995**, *51*, 5824–5831.
[123] Kossyrev, P.A.; Qi, J.; Priezjev, N.V.; Pelcovits, R.A. *Appl. Phys. Lett.* **2002**, *81*, 2986–1–2986–3.
[124] Murashige, T.; Fujikake, H.; Ikehata, S.; Sato, F. *Jpn. J. Appl. Phys.* **2003**, *42*, 1614–1617.
[125] Fan, Y.H.; Ren, H.; Wu, S.T. *Appl. Phys. Lett.* **2003**, *82*, 2945–1–2945–3.
[126] Liao, C.T.; Jiang, M.H.; Wu, N.C.; Wu, Z.L.; Zou, S.F.; Lee, J.Y. *J. Chin. Inst. Eng.* **2010**, *33*, 799–810.
[127] Goodby, J.W.; Waugh, M.A.; Stein, S.M.; Chin, E.; Pindak, R.; Patel, J.S. *J. Am. Chem. Soc.* **1989**, *111*, 8119–8125.
[128] Goodby, J.W.; Waugh, M.A.; Stein, S.M.; Chin, E.; Pindak, R.; Patel, J.S. *Nature (London, UK)* **1989**, *337*, 449–452.
[129] de Gennes, P.G. *Solid State Commun.* **1972**, *10*, 753–756.
[130] Renn, S.R.; Lubensky, T.C. *Phys. Rev. A: At., Mol., Opt. Phys.* **1988**, *38*, 2132–2147.
[131] Srajer, G.; Pindak, R.; Waugh, M.A.; Goodby, J.W. *Phys. Rev. Lett.* **1990**, *64*, 1545–1–1545–4.
[132] Renn, S.R. *Phys. Rev. A: At., Mol., Opt. Phys.* **1992**, *45*, 953–973.

[133] Ihn, K.J.; Zasadzinski, J.A.N.; Pindak, R.; Slaney, A.J.; Goodby, J.W. *Science* **1992**, *258*, 275–278.
[134] Navailles, L.; Barois, P.; Nguyen, H.T. *Phs. Rev. Lett.* **1993**, *71*, 545–548.
[135] Wu, S.L.; Yen, P.C.; Hsieh, W.J. *Liq. Cryst.* **1998**, *24*, 741–746.
[136] Seshadri, T.; Haupt, H.J. *Chem. Commun.* **1998**, 735–736.
[137] Wu, S.L.; You, J.H.; Uang, B.J. *Liq. Cryst.* **2001**, *28*, 69–75.
[138] Bayón, R.; Coco, S.; Espinet, P. *Chem. Mater.* **2002**, *14*, 3515–3518.
[139] Cha, S.W.; Jin, J.I.; Achard, M.F.; Hardiyub, F. *Liq. Cryst.* **2002**, *29*, 755–763.
[140] Goodby, J.W. *Curr. Opin. Colloid Interface Sci.* **2002**, *7*, 326–332.
[141] Kramarenko, N.L.; Kulishovs, V.I.; Kutulya, L.A.; Semenkova, G.P.; Seminozhenko, V.P.; Shkolnikova, N.I. *Liq. Cryst.* **1997**, *22*, 535–541.
[142] Pollmann, P.; Stegemeyer, H. *Liq. Cryst.* **1999**, *26*, 1845–1848.
[143] Dierking, I. *Liq. Cryst.* **2001**, *28*, 165–170.
[144] Dhar, R.; Pandey, M.B.; Agrawal, V.K. *Phase transitions* **2003**, *76*, 763–780.
[145] Dhar, R.; Srivastava, A.K.; Agrawal, V.K. *Phase transitions* **2003**, *76*, 959–974.
[146] Renn, S.R.; Lubensky, T.C. *Mol. Cryst. Liq.Cryst.* **1991**, *209*, 349–355.
[147] Renn, S.R. *Phys. Rev. A: At., Mol., Opt. Phys.* **1992**, *45*, 953–973.
[148] Dierking, I. *Textures of Liquid Crystals*; Wiley-VCH: Weinheim, 2003.
[149] Nguyen, H.T.; Bouchta, A.; Navailles, L.; Barois, P.; Isaert, N.; Twieg, R.J.; Maaroufi, A.; Destrade, C. *J. Phys. II France* **1992**, *2*, 1889–1906.
[150] Navailles, L.; Barois, P.; Nguyen, H.T. *Phys. Rev. Lett.* **1993**, *71*, 545–1–545–4.
[151] Schacht, J.; Baethge, H.; Giesselmann, F.; Zugenmaier, P. *J. Mater. Chem.* **1998**, *8*, 603–612.
[152] Dierking, I.; Lagerwall, S.T. *Liq. Cryst.* **1999**, *26*, 83–95.
[153] Li, M.H.; Laux, V.; Nguyen, H.T.; Sigaud, G.; Barois, P.; Isaert, N. *Liq. Cryst.* **1997**, *23*, 389–408.
[154] Young, M.; Pitsi, G.; Li, M.H.; Nguyen, H.T.; Jamee, P.; Sigaud, G.; Thoen, J. *Liq. Cryst.* **1998**, *25*, 387–391.
[155] Yelamaggad, C.V.; Bonde, N.L.; Achalkumar, A.S.; Shankar Rao, D.S.; Krishna Prasad, S.; Prajapati, A.K. *Chem. Mater.* **2007**, *19*, 2463–2472.
[156] Pandey, M.B.; Dhar, R. *J. Indian Inst. Sci.* **2009**, *89*, 147–167.
[157] Lubensky, T.C. *Physica A* **1995**, *220*, 99–112.
[158] Hu, Y.; Martinez-Miranda, L.J. *Mater. Res. Soc. Symp. Proc.* **1999**, *543*, 201–205.
[159] Shankar Rao, D.S.; Prasad, S.K.; Raja, V.N.; Yelamaggad, C.V.; Anitha Nagamani, S. *Phys. Rev. Lett.* **2001**, *87*, 0855041–1–085504–4.
[160] Cha, S.W.; Jin, J.I.; Achard, M.F.; Hardouin, F. *Liq. Cryst.* **2002**, *29*, 755–763.
[161] Shubashree, S.; Sadashiva, B.K. *Curr. Sci.* **2003**, *85,* 1061–1065.
[162] Manjuladevi, V.; Madhusudana, N.V. *Liq. Cryst.* **2005**, *32*, 1071–1076.
[163] Yelamaggad, C.V.; Shashikala, I.S.; Hiremath, U.S.; Rao, D.S.S.; Prasad, S.K. *Liq. Cryst.* **2007**, *34*, 153–167.
[164] Gupta, M.; Vaid, R.; Gupta, V.; Bamezai, R.K. *Indian J. Chem.* **2008**, *47A*, 1512–1515.
[165] Pandey, M.B.; Dhar, R.; Achalkumar, A.S.; Yelamaggad, C.V. *Phase Transitions* **2008**, *81*, 449–458.
[166] Yelamaggad, C.V.; Shanker, G. *Tetrahedron* **2008**, *64*, 3760–3761.
[167] Majumdar, K.C.; Kumar Sinha, R.; Chakravorty, S. *J. Phys. Chem. Solids.* **2009**, *70*, 1171–1174.
[168] Majumdar, K.C.; Chakravorty, S.; Pal, N.; Rao, N.V.S. *Tetrahedron* **2009**, *65*, 152–157.
[169] Garoff, S.; Meyer, R.B. *Phys. Rev. Lett.* **1977**, *38*, 848–1–848–4.
[170] Clark, N.A.; Lagerwall. S.T. *Appl. Phys. Lett.* **1980**, *36*, 899–1–899–3.
[171] Andersson, G.; Dahl, I.; Keller, P.; Kuczyński, W.; Lagerwall, S.T.; Skarp, K.; Stebler, B. *Appl. Phys. Lett.* **1987**, *51*, 640–1–640–3.
[172] Elston, S.; Sambles, R. *The Optics of Thermotropic Liquid Crystals*; Taylor and Francis: London, 1998.
[173] Spector, M.S.; Heiney, P.A.; Naciri, J.; Weslowski, B.T.; Holt, D.B.; Shashidhar, R. *Phys. Rev. E: Stat., Nonlinear, Soft Matter Phys.* **2000**, *61*, 1579–1584.
[174] Have, K.D.; Dahlgren, A.; Rudquist, P.; Lagerwall, J.P.F.; Andersson, G.; Matuszczyk, M.; Lagerwall, S.T.; Dabrowski, R.; Drzewinski, W. *Ferroelectrics* **2000**, *244*, 415–428.
[175] Clark, N.A.; Bellini, T.; Shao, R.F.; Coleman, D.; Bardon, S.; Link, D.R.; Maclennan, J.E. *Appl. Phys. Lett.* **2002**, *80*, 4097–1–4097–3.
[176] Galli, G.; Reihmann, M.; Crudeli, A.; Chiellini, E.; Panarin, Y.; Vij, J.; Blanc, C.; Lorman, V.; Olsson, N. *Mol. Cryst. Liq. Cryst.* **2005**, *439*, 2111–2123.
[177] Spurce, G.; Pringle, R.D. *Mol. Cryst. Liq. Cryst.* **1988**, *154*, 307–321.
[178] Yeh, P.; Gu, C. *Optics of Liquid Crystal Displays*; John Wiley and Sons: New York, 1999.
[179] de Gennes, P.G.; Prost, J. *The Physics of Liquid Crystals*; Clarendon: Oxford, 1993.
[180] Schiekel, M.F.; Fahrenschon, K. *Appl. Phys. Lett.* **1971**, *19*, 391–1–391–3.
[181] Hareng, M.; Assouline, G.; Leiba, E. *Electron. Lett.* **1971**, *7*, 699–700.
[182] Hareng, M.; Assouline, G.; Leiba, E. *Proc. IEEE* **1972**, *60*, 913–914.
[183] Lackner, A.M.; Margerum, J.D.; Miller, L.J.; Smith, W.H. *Proc. SID* **1990**, *31*, 321–326.
[184] Kundu, S.K.; Okabe, E.; Haase, W.; Chaudhuri, B.K. *Phys. Rev. E: Stat., Nonlinear, Soft Matter Phys.* **2001**, *64*, 051708–1–051708–9.
[185] Kundu, S.K.; Chaudhuri, B.K.; Seed, A.; Ja'kli, A. *Phys. Rev. E: Stat., Nonlinear, Soft Matter Phys.* **2003**, *67*, 041704–1–041704–5.
[186] Kaur, S.; Thakur, A.K.; Chauhan, R.; Bawa, S.S.; Biradar, A.M. *J. Appl. Phys.* **2004**, *96*, 2547–2551.
[187] Ho, C.Y.; Lee, J.Y. *J. Appl. Polym. Sci.* **2006**, *100*, 1688–1704.
[188] Mukherjee, A.; Rahman, M.; Bhattacharyya, S.S.; Chaudhuri, B.K.; Yoshizawa, A. *Chem. Phys. Lett.* **2007**, *443*, 71–75.
[189] Liang, H.H.; Xiao, Y.Z.; Hsh, F.J.; Wu, C.C.; Lee, J.Y. *Liq. Cryst.* **2010**, *37*, 255–261.
[190] Ho, C.Y.; Chang, C.C.; Lee, J.Y. *J. Appl. Polym. Sci.* **2010**, *117*, 3454–3459.

[191] Liao, C.T.; Wu, Z.L.; Wu, N.C.; Liu, J.Y.; Zou, S.F.; Lee, J.Y. *Mol. Cryst. Liq. Cryst.* **2010**, *533*, 3–15.
[192] Liao, C.T.; Liu, J.Y.; Jiang, M.H.; Zou, S.F.; Wu, N.C.; Wu, Z.L.; Lee, J.Y. *Mol. Cryst. Liq. Cryst.* **2010**, *533*, 115–125.
[193] Liao, C.T.; Lee, J.Y.; Lai, C.C. *Mol. Cryst. Liq. Cryst.* **2011**, *534*, 1–16.
[194] Liao, C.T.; Lee, J.Y.; Lai, C.C. *Mol. Cryst. Liq. Cryst.* **2011**, *534*, 91–109.
[195] Li, X.T.; Kawakami, A.; Akiyama, H.; Kobayashi, S.; Iimura, Y. *Jpn. J. Appl. Phys.* **1998**, *37*, L743–L745.
[196] Nastishin, Y.A.; Polak, R.D.; Shiyanovskii, S.V. *Appl. Phys. Lett.* **1999**, *75*, 202–1–202–3.
[197] Ito, T.; Nakanishi, K.; Nishikawa, M.; Yokoyama, Y.; Takeuchi, Y. *J. Poly.* **1995**, *27*, 240–246.
[198] Miller, W.J.; Abbott, N.L. *Langmuir* **1997**, *13*, 7106–7114.
[199] Ge, J.J.; Li, C.Y.; Xue, G.; Mann, I.K.; Zhang, D.; Wang, S.Y.; Harris, F.W.; Cheng, S.Z.D.; Hong, S.C.; Zhuang, X.; Shen, Y.R. *J. Am. Chem. Soc.* **2001**, *123*, 5678–5776.
[200] Byoung, H.H.; Han, J.A.; Soon, J.R.; Soo, S.C.; Hong, K.B. *Langmuir* **2009**, *25*, 8306–8312.
[201] Chiang, C.H.; Tzeng, S.Y.T.; Sie, F.C.; Huang, R.H.; Wu, P.C.; Wu, J.J.; Lin, T.Y.; Liu, A.S.; Hsu, L.H.; Liau, W.L.; Len, S.C. *Jpn. J. Appl. Phys.* **2007**, *46*, 5917–5919.
[202] Jakeman, E.; Raynes, E.P. *Phys. Lett.* **1972**, *39A*, 69–70.
[203] Nie, X.; Xianyu, H.; Lu, R.; Wu, T.X.; Wu, S.T. *J. Display Technol.* **2007**, *3*, 280–283.
[204] Jiao, M.; Ge, Z.; Song, Q.; Wu, S.T. *Appl. Phys. Lett.* **2008**, *92*, 061102–1–061102–3.